A posteriori error estimation for numerical model reduction in computational homogenization of porous media

(article starts on next page)

SPECIAL ISSUE ARTICLE

WILEY

A posteriori error estimation for numerical model reduction in computational homogenization of porous media

Fredrik Ekre | **Fredrik Larsson** | **Kenneth Runesson** | **Ralf Jänicke**

Department of Industrial and Materials Science, Chalmers University of Technology, Gothenburg, Sweden

Correspondence
Fredrik Ekre, Department of Industrial and Materials Science, Chalmers University of Technology, Gothenburg SE-41296, Sweden.
Email: fredrik.ekre@chalmers.se

Summary
Numerical model reduction is adopted for solving the microscale problem that arizes from computational homogenization of a model problem of porous media with displacement and pressure as unknown fields. A reduced basis is obtained for the pressure field using (i) spectral decomposition (SD) and (ii) proper orthogonal decomposition (POD). This strategy has been used in previous work—the main contribution of this article is the extension with an a posteriori estimator for assessing the error in (i) energy norm and in (ii) a given quantity of interest. The error estimator builds on previous work by the authors; the novelty presented in this article is the generalization of the estimator to a coupled problem, and, more importantly, to accommodate the estimator for a POD basis rather than the SD basis. Guaranteed, fully computable and low-cost bounds are derived and the performance of the error estimates is demonstrated via numerical results.

KEYWORDS
computational homogenization, error control, model reduction

1 | INTRODUCTION

Multiscale modeling with computational homogenization is a well-known approach for material modeling. The advantage that multiscale strategies have over direct numerical simulation (DNS) is the reduced computational cost, while still being able to take small scale processes and structures into account. A standard method for multiscale modeling is the so-called finite element squared (FE[2]) procedure, where subscale computations are carried out on representative volume elements (RVE) in each point of the macroscale domain[1] in a nested iteration scheme. Compared with DNS, FE[2] introduces a "model error" due to the smoothing, which was quantified in, e.g. the work of Larsson and Runesson.[1,2]

Even though there are benefits with FE[2] over DNS, the FE[2] scheme can still be very computationally demanding for practical problems, especially for fine macroscale meshes in three dimensions, since the number of RVE problems rapidly increases with the mesh density. It is therefore of interest to reduce the computational cost of solving the individual RVE problems. A number of methods, here denoted numerical model reduction[2] (NMR), have been proposed for reducing the solution space of a discrete RVE problem. In particular, we highlight methods based on superposition of "modes" that

---

[1]In practice one RVE solution per macroscale quadrature point in a finite element setting.
[2]The terms reduced order modeling (ROM) and model order reduction (MOR) are also used frequently in literature. We have chosen to use the term NMR to emphasize that we are using numerical methods to reduce the numerical problem, rather than tampering with the underlying model.

are characteristic to the solution field. Various attempts have been made, in the context of small strain (visco)plasticity, to approximate the inelastic strains by "inelastic modes." One example is the "eigendeformation-based-reduced-order homogenization" technique introduced by Fish and coworkers,[3,4] which relies on the concept of transformation field analysis, originally proposed by Dvorak and Benveniste.[5] Michel and Suquet[6,7] proposed a similar approach coined nonuniform transformation field analysis (NTFA). Fritzen et al[8-11] exploited NTFA combined with proper orthogonal decomposition (POD) for viscoelasticity and a class of standard dissipative materials. Jänicke et al[12] applied this approach to poroelasticity, whereby the pore pressure plays a role similar to inelastic strains in the NTFA framework. As a consequence of the reduced model, the macroscale problem reduces to a single-phase continuum, where the "mode coefficients" can be interpreted as internal variables. This is the reduction model that is considered in this article. Other reduction techniques have been studied in the context of multiscale finite element methods by, e.g. Nguyen[13] for parametrized PDEs and by Efendiev et al[14,15] for flows in heterogeneous media. The concept of "hyperreduction" has also been investigated for multiscale methods by, e.g. Hernández et al[16] and Memarnahavandi et al,[17] where, in addition to reducing of the number of degrees of freedom, also the cost for evaluating the residual is reduced.

Naturally the use of a reduced basis results in an additional source of error, and therefore it is of interest to control and quantify this error. Several different error estimators have been developed, for different model reduction techniques, in the context of multiscale modeling. Methods for estimating the error from POD type reduction techniques have been presented by Abdulle et al[18,19] for heterogeneous multiscale methods and by Boyaval[20] for numerical homogenization. Ohlberger and Schindler developed a method for estimating the error for localized reduced basis multiscale methods. Error estimation based on the constitutive relation error has been proposed by Kerfriden et al[21] and Chamoin and Legoll.[22] For the estimator proposed in this article, we consider the fully resolved finite element solution to be the exact one, similar to what was presented in Aggestam et al[23] and Ekre et al.[24] The consequence of this is that the estimator only quantifies the error stemming from the use of a reduced base and "ignores" e.g. space and time discretization errors. Naturally it would be of interest to develop an estimator which quantifies these errors as well. However, there are cases where the point of departure is already a fine mesh; it might, for example, be obtained from detailed voxel data or be required to capture complex microstructural features. In addition, for linear problems, many of the necessary quantities can be precomputed in an "offline" stage where one can afford the fine mesh without having to tackle the problem of integration, as one would have to do for, e.g. a nonlinear problem.

In this article, we consider a continuum mechanics model of porous media as the model problem, following the work in Jänicke et al.[12] We will consider two different methods of obtaining a reduced basis for the microscale problem; spectral decomposition (SD), which was used for the linear transient heat flow problem in, e.g., Aggestam et al,[23] Ekre et al,[24] and POD, which was used for the same porous media problem in Reference 12. The main new contribution of this article, as compared with Jänicke et al,[12] is the extension with an a posteriori error estimator for assessing the accuracy of the reduced solution. We utilize the linearity of the problem and derive an auxiliary symmetric form, cf. e.g. Pares et al.[25-27] From the auxiliary form we obtain error bounds based on the discrete residual, cf. e.g. Jakobsson et al.[28] We aim for guaranteed, explicit, fully computable, bounds on the error introduced by the reduced basis in terms of (i) energy norm and (ii) a user-defined quantity of interest using goal oriented error estimation, cf. Oden and Prudhomme.[29] We aim to base the estimate on the "active" modes, that is, the modes used for the reduced solution, and will thus not consider hierarchical approaches (eg, by computing additional modes used solely for the purpose of estimating the error). This strategy for estimating the error follows what was presented in References 23,24. The novelty in this article is the generalization of the estimator. They key differences can be summarized as follows; the estimator is derived for a POD basis (rather than for a SD basis), the estimator is generalized for the coupled problem, the implicit relation between pressure and displacement (via static equilibrium) is used to eliminate the displacement field from the pertinent error equations.

Throughout this article, regular font is used to denote scalars (eg, α), bold italic font is used to denote first- and second-order tensors (eg, $\boldsymbol{u}$, $\boldsymbol{\varepsilon}$), and bold font to denote fourth-order tensors (eg, **E**). The scalar product (single contraction) is denoted by $\cdot$, double contraction is denoted with : and the outer product denoted by $\otimes$. For first-order tensors $\boldsymbol{a}$, $\boldsymbol{b}$, second-order tensor $\boldsymbol{A}$ and fourth-order tensor **B**, we thus have

$$\boldsymbol{a} \cdot \boldsymbol{b} = a_i b_i, \tag{1a}$$

$$(\boldsymbol{A} \cdot \boldsymbol{b})_i = A_{ij} b_j, \tag{1b}$$

$$(\mathbf{B} : \boldsymbol{A})_{ij} = B_{ijkl} A_{kl}, \tag{1c}$$

$$(\boldsymbol{a} \otimes \boldsymbol{b})_{ij} = a_i b_j, \tag{1d}$$

for Cartesian components, where repeated indices are summed over (Einstein summation convention). A superposed dot is used for time derivatives (eg, $\dot{u} = \frac{\mathrm{d}u}{\mathrm{d}t}$). Volume averaging of a field $\bullet$ is denoted as

$$\langle \bullet \rangle_\square := \frac{1}{|\Omega_\square|} \int_{\Omega_\square} \bullet \, \mathrm{d}\Omega, \tag{2}$$

where $\Omega_\square$ is the domain occupied by an RVE, and $|\Omega_\square|$ the corresponding volume.

This article is outlined as follows: Section 2 introduces computational homogenization, for the model problem of porous media. Section 3 introduces NMR and describes how it is applied to the microscale (RVE) problem(s). Section 4 discusses how the error in the reduced solution can be estimated in terms of an energy norm, and Section 5 describes the goal oriented error estimation. Section 6 presents numerical results for two example problems, which verify the error estimates. This article is concluded in Section 7, which summarizes the findings.

2 | TWO-SCALE ANALYSIS BASED ON COMPUTATIONAL HOMOGENIZATION

2.1 | The model problem—Strong and space-time weak formats

As a model problem, we consider a continuum mechanics description of a linear-elastic porous medium, where the pores are filled with a viscous fluid. We base our model on Jänicke et al[12] which adapts Biot's equations for linear consolidation,[30,31] with displacement $\boldsymbol{u} = \boldsymbol{u}(\boldsymbol{x}, t)$ and pressure $p = p(\boldsymbol{x}, t)$ as the primary fields

$$-\boldsymbol{\sigma}(\boldsymbol{u}, p) \cdot \boldsymbol{\nabla} = \boldsymbol{0} \qquad \forall \boldsymbol{x} \in \Omega \times (0, T], \tag{3a}$$

$$\dot{\Phi}(\boldsymbol{u}, p) + \boldsymbol{\nabla} \cdot \boldsymbol{w}(\boldsymbol{\nabla} p) = 0 \qquad \forall \boldsymbol{x} \in \Omega \times (0, T], \tag{3b}$$

where $\boldsymbol{\sigma}$ is the linear stress tensor, Φ the fluid storage function and $\boldsymbol{w}$ the seepage velocity. The two fields are subjected to standard boundary conditions on the Dirichlet ($\Gamma_D^{(u|p)}$) and Neumann ($\Gamma_N^{(u|p)}$) parts of the boundary, respectively

$$\boldsymbol{u} = \boldsymbol{u}^{\mathrm{pres}} \quad \text{on } \Gamma_D^{(u)} \times (0, T], \quad \boldsymbol{t} := \boldsymbol{\sigma} \cdot \boldsymbol{n} = \boldsymbol{t}^{\mathrm{pres}} \quad \text{on } \Gamma_N^{(u)} \times (0, T], \tag{4a}$$

$$p = p^{\mathrm{pres}} \quad \text{on } \Gamma_D^{(p)} \times (0, T], \quad h := \boldsymbol{w} \cdot \boldsymbol{n} = h^{\mathrm{pres}} \quad \text{on } \Gamma_N^{(p)} \times (0, T]. \tag{4b}$$

For simplicity, we will consider linear constitutive relations for the stress, fluid storage, and fluid flux. The stress is given by

$$\boldsymbol{\sigma} = \mathbf{E} : \boldsymbol{\varepsilon}[\boldsymbol{u}] - \alpha p \boldsymbol{I}, \tag{5}$$

where $\mathbf{E}$ is the constant elastic stiffness tensor, $\boldsymbol{\varepsilon}[\boldsymbol{u}] = [\boldsymbol{u} \otimes \boldsymbol{\nabla}]^{\mathrm{s}}$ is the linear strain tensor and α is the so-called Biot's coefficient. The storage function and seepage velocity for the liquid phase are given by

$$\Phi = \phi + \alpha \boldsymbol{\nabla} \cdot \boldsymbol{u} + \beta p, \tag{6a}$$

$$\boldsymbol{w} = -\boldsymbol{K} \cdot \boldsymbol{\nabla} p, \tag{6b}$$

where ϕ is the (initial) porosity, $\boldsymbol{K} = k\boldsymbol{I}$ is the permeability tensor with isotropic permeability k, and β is the compressibility parameter of the fluid-filled pore space. α and β are defined in terms of the bulk moduli of the fluid, K^{f}, and the solid, K^{s}, phase as follows:

$$\alpha = 1 - \frac{K}{K^{\mathrm{s}}}, \tag{7a}$$

$$\beta = \frac{\phi}{K^{\mathrm{f}}} + \frac{\alpha - \phi}{K^{\mathrm{s}}}. \tag{7b}$$

Finally, we need an initial condition for Φ, viz.

$$\Phi|_{t=0} = \Phi_0 = \phi + \alpha \nabla \cdot \boldsymbol{u}_0 + \beta p_0. \tag{8}$$

The standard weak format in space-time, corresponding to (3), reads: Find $(\boldsymbol{u}, p) \in \mathcal{U} \times \mathcal{P}$ such that

$$\iint_I \int_\Omega \left[\varepsilon[\boldsymbol{v}] : \mathbf{E} : \varepsilon[\boldsymbol{u}] - \nabla \cdot \boldsymbol{v}\, \alpha p \right] \mathrm{d}\Omega \mathrm{d}t = \iint_I \int_{\Gamma_{\mathrm{N}}} \boldsymbol{v} \cdot \boldsymbol{t}^{\mathrm{pres}} \mathrm{d}\Gamma \mathrm{d}t \quad \forall \boldsymbol{v} \in \mathcal{V}, \tag{9a}$$

$$\iint_I \int_\Omega [q\beta \dot{p} + \nabla q \cdot \boldsymbol{K} \cdot \nabla p + \nabla \cdot \dot{\boldsymbol{u}}\, \alpha q] \mathrm{d}\Omega \mathrm{d}t + \int_\Omega [q\Phi]|_{t=0} \mathrm{d}\Omega$$
$$= \iint_I \int_{\Gamma_{\mathrm{N}}} q h^{\mathrm{pres}} \mathrm{d}\Gamma \mathrm{d}t + \int_\Omega [q\Phi_0]|_{t=0} \mathrm{d}\Omega \quad \forall q \in \mathcal{Q}. \tag{9b}$$

The semidiscrete version of (9) is obtained by defining

$$\mathbb{U}(t) := \left\{ \boldsymbol{v} \in \mathbb{U}_{\mathrm{h}} : \boldsymbol{v} = \boldsymbol{u}^{\mathrm{pres}} \text{ on } \Gamma_{\mathrm{D}}^{(u)} \right\}, \tag{10a}$$

$$\mathbb{U}^0 := \left\{ \boldsymbol{v} \in \mathbb{U}_{\mathrm{h}} : \boldsymbol{v} = \boldsymbol{0} \text{ on } \Gamma_{\mathrm{D}}^{(u)} \right\}, \tag{10b}$$

$$\mathbb{P}(t) := \left\{ q \in \mathbb{P}_{\mathrm{h}} : q = p^{\mathrm{pres}} \text{ on } \Gamma_{\mathrm{D}}^{(p)} \right\}, \tag{10c}$$

$$\mathbb{P}^0 := \left\{ q \in \mathbb{P}_{\mathrm{h}} : q = 0 \text{ on } \Gamma_{\mathrm{D}}^{(p)} \right\}, \tag{10d}$$

where $\mathbb{U}_{\mathrm{h}} \in [H^1(\Omega)]^3$ and $\mathbb{P}_{\mathrm{h}} \in H^1(\Omega)$ represents the finite element discretization, and H^1 the space of functions with square integrable derivatives of order 0 and 1. The spaces used in (9) are consequently defined as

$$\mathcal{U} := H^1\left(I; \mathbb{U}(t)\right), \tag{11a}$$

$$\mathcal{V} := L_2\left(I; \mathbb{U}^0\right), \tag{11b}$$

$$\mathcal{P} := H^1\left(I; \mathbb{P}(t)\right), \tag{11c}$$

$$\mathcal{Q} := \left\{ q(\boldsymbol{x}, t) : q|_{t=0} \in \mathbb{P}^0, q|_I \in L_2\left(I; \mathbb{P}^0\right) \right\}. \tag{11d}$$

Here, we introduced Bochner spaces for space-time functions, such that, for example, $H^1(I; X) = \{v(\boldsymbol{x}, t) : \|v(\bullet, t)\|_X \in H^1(I)\}$ and $L_2(I; X) = \{v(\boldsymbol{x}, t) : \|v(\bullet, t)\|_X \in L_2(I)\}$ for a space X of spatial functions with suitable norm $\| \bullet \|_X$. $L_2(I)$ and $H^1(I)$ are the spaces of square integrable functions and functions of square integrable derivatives, respectively, on the time interval I.

Remark 1. In order to shorten notation, we henceforth adopt the convention that the trace is included in $H^1(I)$, meaning that, for example, $q \in H^1(I; \mathbb{X})$ infers that $q(0)$ and $q(T)$ exist and reside in $\mathbb{X}$. $\square$

2.2 | First-order selective homogenization in the spatial domain

The single-scale problem in Subsection 2.1 is replaced by a two-scale problem. We introduce (i) running averages in the weak form and (ii) scale separation via first-order selective homogenization, following Larsson et al.[32] As a first step, we replace the single-scale problem (9) with the following, two-scale, problem: Find $(\boldsymbol{u}, p) \in \mathcal{U}_{\mathrm{FE}^2} \times \mathcal{P}_{\mathrm{FE}^2}$ such that

$$A^{(u)}(\boldsymbol{u}, p; \boldsymbol{v}) = L^{(u)}(\boldsymbol{v}) \qquad \forall \boldsymbol{v} \in \mathcal{V}_{\mathrm{FE}^2}, \tag{12a}$$

$$A^{(p)}(\boldsymbol{u}, p; q) = L^{(p)}(q) \qquad \forall q \in \mathcal{Q}_{\mathrm{FE}^2}, \tag{12b}$$

where the space-time variational forms are defined as

$$A^{(u)}(\boldsymbol{u}, p; \boldsymbol{v}) \; := \int_I \int_\Omega \Big[\mathfrak{a}_\square^{(u)}(\boldsymbol{u}, \boldsymbol{v}) - \mathfrak{b}_\square(p, \boldsymbol{v}) \Big] \mathrm{d}\Omega \mathrm{d}t, \tag{13a}$$

$$L^{(u)}(\boldsymbol{v}) \; := \int_I \int_{\Gamma_\mathrm{N}} \boldsymbol{v} \cdot \boldsymbol{t}^{\mathrm{pres}} \mathrm{d}\Gamma \mathrm{d}t, \tag{13b}$$

$$A^{(p)}(\boldsymbol{u}, p; q) \; := \int_I \int_\Omega \Big[\mathfrak{m}_\square(\dot{p}, q) + \mathfrak{a}_\square^{(p)}(p, q) + \mathfrak{b}_\square(q, \dot{\boldsymbol{u}}) \Big] \mathrm{d}\Omega \mathrm{d}t + \int_\Omega \Big[\mathfrak{m}_\square(p, q) + \mathfrak{b}_\square(q, \boldsymbol{u}) \Big] |_{t=0} \mathrm{d}\Omega, \tag{13c}$$

$$L^{(p)}(q) \; := \int_I \int_{\Gamma_\mathrm{N}} q h^{\mathrm{pres}} \mathrm{d}\Gamma \mathrm{d}t + \int_\Omega \Big[\mathfrak{m}_\square(p_0, q) + \mathfrak{b}_\square(q, \boldsymbol{u}_0) \Big] |_{t=0} \mathrm{d}\Omega. \tag{13d}$$

In (13), we introduced pertinent space-variational RVE-forms, representing running averages on domains $\Omega_\square$ located at each macroscale spatial point $\overline{\boldsymbol{x}}$:

$$\mathfrak{a}_\square^{(u)}(\boldsymbol{u}, \boldsymbol{v}) \; := \langle \varepsilon[\boldsymbol{v}] : \mathbf{E} : \varepsilon[\boldsymbol{u}] \rangle_\square, \tag{14a}$$

$$\mathfrak{b}_\square(u, \boldsymbol{v}) \; := \langle \boldsymbol{\nabla} \cdot \boldsymbol{v} \, \alpha u \rangle_\square, \tag{14b}$$

$$\mathfrak{m}_\square(u, v) \; := \langle v \beta u \rangle_\square, \tag{14c}$$

$$\mathfrak{a}_\square^{(p)}(u, v) \; := \langle \boldsymbol{\nabla} v \cdot \boldsymbol{K} \cdot \boldsymbol{\nabla} u \rangle_\square. \tag{14d}$$

Remark 2. For later use, we also introduce two norms based on $\mathfrak{m}_\square$ and $\mathfrak{a}_\square^{(p)}$, respectively:

$$\|v\|_\mathfrak{m} \; := \sqrt{\mathfrak{m}_\square(v, v)}, \quad \|v\|_\mathfrak{a} \; := \sqrt{\mathfrak{a}_\square^{(p)}(v, v)}. \tag{15}$$

$\square$

In order to define the two-scale trial spaces $\mathcal{U}_{\mathrm{FE}^2}$, $\mathcal{P}_{\mathrm{FE}^2}$ and the corresponding test spaces $\mathcal{V}_{\mathrm{FE}^2}$, $\mathcal{Q}_{\mathrm{FE}^2}$, we introduce first-order homogenization. However, to simplify matters we adopt *selective* homogenization, in the sense that it is only the displacement field $\boldsymbol{u}$ that is decomposed into macroscale and microscale parts, whereas p is represented only as a fluctuation field. Hence, in each RVE, centered at macroscale coordinate $\overline{\boldsymbol{x}}$, we thus decompose $\boldsymbol{u}$ as

$$\boldsymbol{u}(\overline{\boldsymbol{x}}; \boldsymbol{x}, t) = \boldsymbol{u}^\mathrm{M}(\overline{\boldsymbol{x}}; \boldsymbol{x}, t) + \boldsymbol{u}^\mu(\overline{\boldsymbol{x}}; \boldsymbol{x}, t), \quad (\boldsymbol{x}, t) \in \Omega_\square \times I, \tag{16}$$

where we use first-order homogenization for the macroscale part, viz.

$$\boldsymbol{u}^\mathrm{M}(\overline{\boldsymbol{x}}; \boldsymbol{x}, t) \; := \overline{\boldsymbol{u}}(\overline{\boldsymbol{x}}, t) + \overline{\varepsilon}(\overline{\boldsymbol{x}}, t) \cdot [\boldsymbol{x} - \overline{\boldsymbol{x}}], \tag{17}$$

with $\overline{\varepsilon} \; := [\overline{\boldsymbol{u}} \otimes \boldsymbol{\nabla}]^\mathrm{s}$. As to the pressure field, we have

$$p(\overline{\boldsymbol{x}}; \boldsymbol{x}, t) = p^\mu(\overline{\boldsymbol{x}}; \boldsymbol{x}, t), \quad (\boldsymbol{x}, t) \in \Omega_\square \times I, \tag{18}$$

that is, the pressure field "lives" entirely on the subscale.

We are now in the position to define the two-scale ansatz and test spaces

$$\mathcal{U}_{\mathrm{FE}^2} \; := \Big\{ \boldsymbol{u} : \; \boldsymbol{u}|_{\Omega_\square} = \boldsymbol{u}^\mathrm{M}[\overline{\boldsymbol{u}}] + \boldsymbol{u}^\mu, \; \boldsymbol{u}|_{\Gamma_\mathrm{N}^{(\omega)}} = \overline{\boldsymbol{u}}, \; \boldsymbol{u}^\mu \in \mathcal{U}_\square^\mu, \; \overline{\boldsymbol{u}} \in \overline{\mathcal{u}} \Big\}, \tag{19a}$$

$$\mathcal{V}_{\mathrm{FE}^2} \; := \Big\{ \boldsymbol{v} : \; \boldsymbol{v}|_{\Omega_\square} = \boldsymbol{v}^\mathrm{M}[\overline{\boldsymbol{v}}] + \boldsymbol{v}^\mu, \; \boldsymbol{v}|_{\Gamma_\mathrm{N}^{(\omega)}} = \overline{\boldsymbol{v}}, \; \boldsymbol{v}^\mu \in \mathcal{V}_\square^\mu, \; \overline{\boldsymbol{v}} \in \overline{\mathcal{V}} \Big\}, \tag{19b}$$

$$\mathcal{P}_{\mathrm{FE}^2} := \left\{ p: \ p|_{\Omega_\square} = p^\mu, \ p^\mu \in \mathcal{P}_\square \right\}, \tag{19c}$$

$$\mathcal{Q}_{\mathrm{FE}^2} := \left\{ q: \ q|_{\Omega_\square} = q^\mu, \ q^\mu \in \mathcal{Q}_\square \right\}, \tag{19d}$$

cf. Ekre et al.[24] The details of the ansatz and test spaces in (19) is discussed in the following two sections (2.3 and 2.4).

2.3 | The macroscale (homogenized) problem

The macroscale problem is obtained from Equation (12) by setting $\boldsymbol{v}^\mu = \boldsymbol{0}$ and $q^\mu = 0$. Find $\overline{\boldsymbol{u}} \in \overline{\mathcal{U}}$ such that

$$\int_I \int_\Omega \varepsilon[\overline{\boldsymbol{v}}] : \overline{\boldsymbol{\sigma}}(\overline{\boldsymbol{u}}, \boldsymbol{u}^\mu) \mathrm{d}\Omega \mathrm{d}t = \int_I \int_{\Gamma_{\mathrm{N}}} \overline{\boldsymbol{v}} \cdot \boldsymbol{t}^{\mathrm{pres}} \mathrm{d}\Gamma \mathrm{d}t \quad \forall \overline{\boldsymbol{v}} \in \overline{\mathcal{V}}, \tag{20}$$

where $\overline{\mathcal{U}}$ and $\overline{\mathcal{V}}$ are the ansatz and test spaces for the macroscale problem. We omit the exact definitions of these spaces, since we henceforth in this article focus solely on the local microscale RVE-problem. The homogenized stress $\overline{\boldsymbol{\sigma}}$ is defined as

$$\overline{\boldsymbol{\sigma}}\{\varepsilon[\overline{\boldsymbol{u}}]\} := \langle \boldsymbol{\sigma} \rangle_\square, \tag{21}$$

where $\overline{\boldsymbol{\sigma}}\{\overline{\varepsilon}\}$ is implicit due to the history dependence.

2.4 | The microscale (RVE) problem

Since we shall (in this article) be concerned only with the solution of the RVE-problem, we consider the situation where $\boldsymbol{u}^{\mathrm{M}}$ from (17) is known, i.e. $\overline{\boldsymbol{u}}(t)$ and $\overline{\varepsilon}(t)$ are known functions in time (for the given RVE in question). The problem (12) thus reduces to that of finding $(\boldsymbol{u}^\mu, p) \in \mathcal{U}_\square^\mu \times \mathcal{P}_\square$ that solve

$$A_\square^{(u)}(\boldsymbol{u}^\mu, p; \boldsymbol{v}^\mu) = L_\square^{(u)}(\boldsymbol{v}^\mu) \qquad \forall \boldsymbol{v}^\mu \in \mathcal{V}_\square^\mu, \tag{22a}$$

$$A_\square^{(p)}(\boldsymbol{u}^\mu, p; q) = L_\square^{(p)}(q) \qquad \forall q \in \mathcal{Q}_\square, \tag{22b}$$

where we introduced the RVE space-time variational forms

$$A_\square^{(u)}(\boldsymbol{u}, p; \boldsymbol{v}) := \int_I \left[\mathfrak{a}_\square^{(u)}(\boldsymbol{u}, \boldsymbol{v}) - \mathfrak{b}_\square(p, \boldsymbol{v}) \right] \mathrm{d}t, \tag{23a}$$

$$L_\square^{(u)}(\boldsymbol{v}) := \int_I \mathfrak{a}_\square^{(u)}\left(-\boldsymbol{u}^{\mathrm{M}}, \boldsymbol{v} \right) \mathrm{d}t, \tag{23b}$$

$$A_\square^{(p)}(\boldsymbol{u}, p; q) := \int_I \left[\mathfrak{m}_\square(\dot{p}, q) + \mathfrak{a}_\square^{(p)}(p, q) + \mathfrak{b}_\square(q, \dot{\boldsymbol{u}}) \right] \mathrm{d}t + \left[\mathfrak{m}_\square(p, q) + \mathfrak{b}_\square(q, \boldsymbol{u}) \right]\Big|_{t=0}, \tag{23c}$$

$$L_\square^{(p)}(q) := \int_I \mathfrak{b}_\square\left(q, -\dot{\boldsymbol{u}}^{\mathrm{M}} \right) \mathrm{d}t + \left[\mathfrak{m}_\square(p_0, q) + \mathfrak{b}_\square(q, \boldsymbol{u}_0 - \boldsymbol{u}^{\mathrm{M}}) \right]\Big|_{t=0}. \tag{23d}$$

We adopt Dirichlet boundary conditions, for both $\boldsymbol{u}^\mu$ and p, and the spaces of spatial functions for the RVE problem are consequently defined as

$$\mathbb{U}_\square^0 := \left\{ \boldsymbol{v} \in \mathbb{U}_{\square,\mathrm{h}} : \ \boldsymbol{v} = \boldsymbol{0} \ \text{on} \ \Gamma_\square \right\}, \tag{24a}$$

$$\mathbb{P}_\square := \left\{ q \in \mathbb{P}_{\square,\mathrm{h}} : \ q = 0 \ \text{on} \ \Gamma_\square \right\}, \tag{24b}$$

where $\mathbb{U}_{\square,h}$ and $\mathbb{P}_{\square,h}$ are the (spatially) FE-discretized function spaces. The trial and test spaces in (22) can be expressed as

$$\mathcal{U}_{\square}^{\mu} := H^1\big(I; \mathbb{U}_{\square}^0\big), \tag{25a}$$

$$\mathcal{V}_{\square}^{\mu} := L_2\big(I; \mathbb{U}_{\square}^0\big), \tag{25b}$$

$$\mathcal{P}_{\square} := H^1\big(I; \mathbb{P}_{\square}\big), \tag{25c}$$

$$\mathcal{Q}_{\square} := \big\{ q(\boldsymbol{x}, t) : \; q|_{t=0} \in \mathbb{P}_{\square}, \; q|_I \in L_2\big(I; \mathbb{P}_{\square}\big) \big\}. \tag{25d}$$

3 ⏐ NUMERICAL MODEL REDUCTION

3.1 ⏐ Preliminaries

We will now use the fact that Equation (22a) is time-invariant, and does not contain any time derivatives, of $\boldsymbol{u}$ or p, to reduce the problem further. As a preliminary step, we introduce an implicit reduction of the displacement fluctuation $\boldsymbol{u}^{\mu}$. For any $t \in I$ we define

$$\boldsymbol{u}^{\mu}(t) = \boldsymbol{u}_{\bar{\varepsilon}}^{\mu}(t) + \boldsymbol{u}_p^{\mu}\{p(t)\}, \tag{26}$$

where $\boldsymbol{u}_{\bar{\varepsilon}}^{\mu}(t) \in \mathbb{U}_{\square}^0(t)$ satisfies

$$\mathfrak{a}_{\square}^{(u)}\big(\boldsymbol{u}_{\bar{\varepsilon}}^{\mu}(t), \delta\boldsymbol{u}^{\mu}\big) = \mathfrak{a}_{\square}^{(u)}\big(-\boldsymbol{u}^{\mathrm{M}}(t), \delta\boldsymbol{u}\big) \qquad \forall\delta\boldsymbol{u}^{\mu} \in \mathbb{U}_{\square}^0, \tag{27}$$

and the implicit function $\boldsymbol{u}_p^{\mu}$ is defined from

$$\boldsymbol{u}_p^{\mu}\{q\} := \boldsymbol{u}_p^{\mu} \in \mathbb{U}_{\square}^0 : \; \mathfrak{a}_{\square}^{(u)}\big(\boldsymbol{u}_p^{\mu}, \delta\boldsymbol{u}\big) = \mathfrak{b}_{\square}(q, \delta\boldsymbol{u}) \qquad \forall\delta\boldsymbol{u} \in \mathbb{U}_{\square}^0. \tag{28}$$

In summary, for a given RVE, we use the following decomposition of $\boldsymbol{u}$

$$\boldsymbol{u} = \boldsymbol{u}^{\mathrm{M}} + \boldsymbol{u}^{\mu} = \underbrace{\boldsymbol{u}^{\mathrm{M}} + \boldsymbol{u}_{\bar{\varepsilon}}^{\mu}}_{=: \; \boldsymbol{u}_{\bar{\varepsilon}}} + \boldsymbol{u}_p^{\mu} = \boldsymbol{u}_{\bar{\varepsilon}} + \boldsymbol{u}_p^{\mu}. \tag{29}$$

Remark 3. We note, from (27), that $\boldsymbol{u}_{\bar{\varepsilon}}^{\mu}$ can be directly assessed in terms of unit strain perturbations, that is,

$$\boldsymbol{u}_{\bar{\varepsilon}}^{\mu}(\boldsymbol{x}, t) = \sum_{i,j=1}^{n_{\mathrm{dim}}} \hat{\boldsymbol{u}}_{\bar{\varepsilon}}^{(i,j)}(\boldsymbol{x})\big[\bar{\varepsilon}(t) \; : \; \boldsymbol{e}_i \otimes \boldsymbol{e}_j\big], \tag{30}$$

where the "unit fields" $\hat{\boldsymbol{u}}_{\bar{\varepsilon}}^{(i,j)} \in \mathbb{U}_{\square}^0$ are solved from

$$\mathfrak{a}_{\square}^{(u)}\big(\hat{\boldsymbol{u}}_{\bar{\varepsilon}}^{(i,j)}, \delta\boldsymbol{u}^{\mu}\big) = -\mathfrak{a}_{\square}^{(u)}\big(\boldsymbol{e}_i \otimes \boldsymbol{e}_j \cdot [\boldsymbol{x} - \bar{\boldsymbol{x}}], \delta\boldsymbol{u}^{\mu}\big) \qquad \forall\delta\boldsymbol{u}^{\mu} \in \mathbb{U}_{\square}^0 \qquad i,j = 1, 2, \ldots n_{\mathrm{dim}}. \tag{31}$$

□

With the displacement fluctuation implicitly known from p we can formulate a condensed version of the original problem in (22); Find $p \in \mathcal{P}_{\square}$ such that

$$A_{\square}(p, q) = L_{\square}(q) \qquad \forall q \in \mathcal{Q}_{\square}, \tag{32}$$

where we defined

$$A_\square(q, r) := \int_I \left[\mathfrak{m}_\square(\dot{q}, r) + \mathfrak{a}_\square^{(p)}(q, r) + \mathfrak{b}_\square(r, \boldsymbol{u}_p^\mu\{\dot{q}\}) \right] dt + \left[\mathfrak{m}_\square(q, r) + \mathfrak{b}_\square(r, \boldsymbol{u}_p^\mu\{q\}) \right]\big|_{t=0}, \tag{33a}$$

$$L_\square(q) := \int_I \mathfrak{b}_\square(q, -\dot{\boldsymbol{u}}_{\bar{\epsilon}}) dt + \left[\mathfrak{m}_\square(p_0, q) + \mathfrak{b}_\square(q, \boldsymbol{u}_0 - \boldsymbol{u}_{\bar{\epsilon}}) \right]\big|_{t=0}. \tag{33b}$$

3.2 | NMR-ansatz

We now introduce the concept of NMR with the aim to reduce the computational cost of solving each RVE problem (32). To this end, we construct a reduced spatial basis for the pressure, and define $p_R(\boldsymbol{x},t)$ as the approximation of $p(\boldsymbol{x},t)$ with an expansion using N_R modes

$$p(\boldsymbol{x}, t) \approx p_R(\boldsymbol{x}, t) = \sum_{a=1}^{N_R} p_a(\boldsymbol{x}) \xi_a(t) \in \mathcal{P}_{\square,R} := H^1(I; \mathbb{P}_{\square,R}), \tag{34}$$

where $\{p_a\}_{a=1}^{N_R}$ is a set of linearly independent basis functions that span the reduced RVE space

$$\mathbb{P}_{\square,R} := \text{span}\{p_a\}_{a=1}^{N_R} \subset \mathbb{P}_\square, \tag{35}$$

and where ξ_a are mode "activity coefficients." The identification of the spatial modes p_a will be discussed further in Subsection 3.4.

Remark 4. We note that in the ansatz (34) the aim is to precompute the spatial modes p_a in the "offline" stage, and later solve for the mode activity coefficients in the "online" stage. This is in contrast to other methods, for example, Proper Generalized Decomposition, where both functions are computed in the online stage. □

In order to satisfy (28), and find $\boldsymbol{u}_p^\mu\{p(t)\}$, we make the following ansatz

$$\boldsymbol{u}_{p,R}^\mu(\boldsymbol{x}, t) = \sum_{a=1}^{N_R} \boldsymbol{u}_a^\mu(\boldsymbol{x}) \xi_a(t) \tag{36}$$

where $\boldsymbol{u}_a^\mu(\boldsymbol{x})$ are (spatial) displacement modes and where $\xi_a(t)$ are the *same* mode activity coefficients as those used for the reduced pressure field. The sequence of displacement modes are readily solved from (28). Find $\boldsymbol{u}_a^\mu \in \mathbb{U}_\square$ such that

$$\mathfrak{a}_\square^{(u)}\left(\boldsymbol{u}_a^\mu, \delta\boldsymbol{u}^\mu\right) = \mathfrak{b}_\square(p_a, \delta\boldsymbol{u}^\mu) \qquad \forall \delta\boldsymbol{u}^\mu \in \mathbb{U}_\square^0 \qquad a = 1, 2, \ldots N_R, \tag{37}$$

i.e. one stationary, linear, problem to solve for each mode p_a.

3.3 | Explicit form of the reduced subscale problem

With the approximations from the previous section we can, following the procedure in Jänicke et al,[12] define the reduced equivalent of (22): Find $p_R \in \mathcal{P}_{\square,R}$ such that

$$A_\square(p_R, q_R) = L_\square(q_R) \qquad \forall q_R \in \mathcal{Q}_{\square,R}, \tag{38}$$

where $\mathcal{Q}_{\square,R}$ follows from (25d), with $\mathbb{P}_\square$ replaced by $\mathbb{P}_{\square,R}$. Hence, we can expand the test function q using the spatial pressure modes, i.e. $q_R = \sum_{a=1}^{N_R} p_a \eta_a$, and express (38) explicitly as the problem of finding the mode coefficients $\xi_a(t) \in H^1(I)$, $a = 1, 2, \ldots, N_R$ such that

$$\sum_{a=1}^{N_R} \left[\sum_{b=1}^{N_R} \int_I \eta_a [\mathfrak{m}_\square(p_b, p_a)\dot{\xi}_b + \mathfrak{a}_\square^{(p)}(p_b, p_a)\xi_b + \mathfrak{b}_\square(p_a, \boldsymbol{u}_b^\mu)\dot{\xi}_b] dt + \eta_a(0) \left[\mathfrak{m}_\square(p_b, p_a)\xi_b + \mathfrak{b}_\square(p_a, \boldsymbol{u}_b^\mu)\xi_b \right]\big|_{t=0} \right.$$

$$= \sum_{a=1}^{N_\mathrm{R}} \left[\int_I \eta_a \mathfrak{b}_\square(p_a, -\dot{\boldsymbol{u}}_{\bar{\varepsilon}}) \mathrm{d}t + \eta_a(0) \left[\mathfrak{m}_\square(p_0, p_a) + \mathfrak{b}_\square(p_a, \boldsymbol{u}_0 - \boldsymbol{u}_{\bar{\varepsilon}}) \right] |_{t=0} \right] \qquad \forall \eta_a \in \mathcal{X}, \quad a = 1, 2, .., N_\mathrm{R}, \tag{39}$$

where

$$\mathcal{X} := \{ v(t) : \ v|_{t=0} \in \mathbb{R}, \ v|_I \in L_2(I) \}. \tag{40}$$

Remark 5. Equation (39) can be formulated as a semidiscrete system of size N_R as follows

$$\underline{M} \, \dot{\vec{\xi}} + \underline{K} \, \vec{\xi} = \vec{f}, \tag{41a}$$

$$\underline{M} \, \vec{\xi}^{0} = \vec{f}^{0}, \tag{41b}$$

where

$$(\underline{M})_{ab} = \mathfrak{m}_\square(p_b, p_a) + \mathfrak{b}_\square(p_a, \boldsymbol{u}_b^\mu), \tag{42a}$$

$$(\underline{K})_{ab} = \mathfrak{a}_\square^{(p)}(p_b, p_a), \tag{42b}$$

$$(\vec{f})_a = \mathfrak{b}_\square(p_a, -\dot{\boldsymbol{u}}_{\bar{\varepsilon}}) = \left[\sum_{ij}^{n_\mathrm{dim}} \mathfrak{b}_\square \left(p_a, -\boldsymbol{e}_i \otimes \boldsymbol{e}_j \cdot [\boldsymbol{x} - \bar{\boldsymbol{x}}] - \hat{\boldsymbol{u}}_{\bar{\varepsilon}}^{(i,j)} \boldsymbol{e}_i \otimes \boldsymbol{e}_j \right) \right] : \dot{\bar{\varepsilon}} \tag{42c}$$

$$(\vec{f}^{0})_a = [\mathfrak{m}_\square(p_0, p_a) + \mathfrak{b}_\square(p_a, \boldsymbol{u}_0 - \boldsymbol{u}_{\bar{\varepsilon}})]|_{t=0}. \tag{42d}$$

$\square$

The full two-scale model involves the solution of (reduced) microscale problems (39), typically one for each macroscale quadrature point, in order to find homogenized stress $\bar{\boldsymbol{\sigma}}$ and the sensitivity w.r.t. the macroscale strain $\frac{\partial \bar{\sigma}}{\partial \bar{\varepsilon}}$. In particular, the homogenized stress can be formulated as

$$\bar{\boldsymbol{\sigma}}(t) = \overline{\mathbf{E}}_{\bar{\varepsilon}} : \boldsymbol{\varepsilon}(t) + \sum_{a=1}^{N_\mathrm{R}} \overline{\boldsymbol{E}}_{p,a} \, \xi_a(t), \tag{43}$$

where the fourth-order tensor $\overline{\mathbf{E}}_{\bar{\varepsilon}}$ and the second-order tensors $\overline{\boldsymbol{E}}_{p,a}$ can be computed in the "offline stage," resulting in efficient evaluation of the homogenized stress, i.e.

$$\overline{\mathbf{E}}_{\bar{\varepsilon}} = \langle \mathbf{E} \rangle_\square + \sum_{ij}^{n_\mathrm{dim}} \left\langle \boldsymbol{E} : \varepsilon \left[\hat{\boldsymbol{u}}_{\bar{\varepsilon}}^{(i,j)} \right] \right\rangle_\square \boldsymbol{e_i} \otimes \boldsymbol{e_j}, \tag{44a}$$

$$\overline{\boldsymbol{E}}_{p,a} = \langle \mathbf{E} : \varepsilon [u_a^\mu] \rangle_\square - \langle \boldsymbol{p_a} \rangle_\square \boldsymbol{I}, \tag{44b}$$

where $\mathbf{E}$ is the fourth-order stiffness tensor for linear elasticity.

3.4 | Construction of the reduced basis

In the previous section, we set aside the discussion about the construction of the spatial modes p_a for the reduced basis. We merely mentioned that the modes span the reduced pressure space $\mathbb{P}_{\square,\mathrm{R}} \subset \mathbb{P}_\square$. In this section, we will briefly discuss two different methods to construct the reduced base: POD and SD.

3.4.1 | Proper orthogonal decomposition

In order to construct a POD basis for the pressure, we collect N_S pressure "snapshots" $\hat{p}_k := p(t_k), k = 1, 2, . . ., N_\mathrm{S}$, in time, from the solution of the fully resolved problem given in Equation (22). To extract modes from the dataset of

snapshots, we first form the correlation matrix $\underline{C}$ with entries

$$(\underline{C})_{kl} = \langle \hat{p}_k \hat{p}_l \rangle_{\square} \quad k, l = 1, 2, \ldots, N_S, \tag{45}$$

which we use to solve the eigenvalue problem $\underline{C}\vec{\varphi} = \lambda \vec{\varphi}$, and obtain eigenvalues λ_a and eigenvectors $\vec{\varphi}_a$, ordered based on the eigenvalues in decreasing order such that $\lambda_1 \geq \lambda_2, \ldots$. The final modes, used for the reduced pressure solution, are finally computed as

$$p_a = \sum_{k=1}^{N_S} \hat{p}_k (\vec{\varphi}_a)_k, \quad a = 1, 2, \ldots, N_R^{POD}. \tag{46}$$

Remark 6. The number of modes N_R^{POD} is determined by truncation of the eigenvalues series, in practice when the quotient λ_N / λ_1 becomes "sufficiently small." $\qquad \square$

3.4.2 | Spectral decomposition

SD is a well suited method of finding a reduced basis for linear problems. In the context of computational homogenization, a spectral base was used for the transient heat flow problem in Aggestam et al[23] for the RVE problem, and later extended to the full two-scale model in Ekre et al.[24] The problem discussed in this article is not well suited for SD, due to the coupling between the two fields. Nevertheless, it is possible to construct a generalized eigenvalue problem from the uncoupled version by simply ignoring the term $\mathfrak{b}_{\square}(\bullet, \bullet)$ in Equation (22b). Find the eigenpairs $(p_a, \lambda_a) \in \mathbb{P}_{\square} \otimes \mathbb{R}^+$ such that

$$\mathfrak{a}_{\square}^{(p)}(p_a, \delta p) = \lambda_a \mathfrak{m}_{\square}(p_a, \delta p) \qquad \forall \delta p \in \mathbb{P}_{\square} \qquad a, b = 1, 2, \ldots, \tag{47a}$$

$$\mathfrak{m}_{\square}(p_a, p_b) = \delta_{ab} \qquad a, b = 1, 2, \ldots, \tag{47b}$$

where $\lambda_1 \leq \lambda_2 \leq \ldots$ are the eigenvalues, and $p_1, p_2, \ldots$ the corresponding eigenfunctions. From (47), we also obtain the standard orthogonality condition

$$\mathfrak{a}_{\square}^{(p)}(p_a, p_b) = \lambda_a \delta_{ab} \qquad a, b = 1, 2, \ldots. \tag{48}$$

The spectral base is not expected to perform particularly well, since it originates from a modified problem which does not take the coupling into account. However, the spectral base is advantageous for the error estimation, as will be discussed in Sections 4 and 5 and may serve as a "reference solution."

3.4.3 | Projection onto the reduced space

For the subsequent error analysis, we define a projection operator $\Pi_R : L_2(\Omega_{\square}) \to \mathbb{P}_{\square,R}$ such that, for any given $q \in L_2(\Omega_{\square})$ and for any given reduced set $\mathbb{P}_{\square,R}$, the projection $\Pi_R q \in \mathbb{P}_{\square,R}$ is defined by the identity

$$\mathfrak{m}_{\square}(\Pi_R q, \delta q) = \mathfrak{m}_{\square}(q, \delta q) \qquad \forall \delta q \in \mathbb{P}_{\square,R}. \tag{49}$$

We also define the complementary operator

$$\Pi_C := I - \Pi_R \tag{50}$$

where I is the identity operator. We note that for $p, q \in L_2(\Omega_{\square})$ the following identity holds

$$\mathfrak{m}_{\square}(p, \Pi_C q) = \mathfrak{m}_{\square}(\Pi_C p, q) \tag{51}$$

since

$$m_\square(p, \Pi_C q) \overset{(50)}{=} m_\square(p, q) - m_\square(p, \Pi_R q)$$

$$\overset{(49)}{=} m_\square(p, q) - m_\square(\Pi_R p, \Pi_R q) \overset{(49)}{=} m_\square(p, q) - m_\square(\Pi_R p, q) \overset{(50)}{=} m_\square(\Pi_C p, q). \tag{52}$$

4 | ESTIMATION OF THE NMR ERROR IN ENERGY NORM

4.1 | Preliminaries

It is clear that the reduced solution p_R is an approximation of p, and that the reduction introduces an error. In this section, we will assess the accuracy of the (reduced) solution by estimating the error. The goal is to obtain an estimate for the error in terms of an energy norm, and in terms of user-defined quantities (goal oriented estimation). We recognize that the total error have multiple sources, in particular (i) NMR and (ii) space and time discretization. In this article, we focus solely on the error from NMR, and thus assume that the resolution in time and space is sufficiently good.

The (exact) error in the pressure is defined as

$$g(\boldsymbol{x}, t) := p(\boldsymbol{x}, t) - p_R(\boldsymbol{x}, t) \quad \in \mathcal{P}_\square, \tag{53}$$

where $p \in \mathcal{P}_\square$ is the exact solution, and where $p_R \in \mathcal{P}_{\square,R}$ is the reduced solution. In order to find an estimate for g we use the following "building blocks":

- definition of the error equation and corresponding residual (Subsection 4.2);
- definition of an auxiliary error equation based on the construction of an auxiliary bilinear form in space-time with associated norm, cf. the work of Parés et al[27] (Subsection 4.3);
- formulation of the explicit energy norm estimate, cf. the work of Jakobsson et al[28] (Subsection 4.4).

This strategy follows the procedure outlined in Aggestam et al,[23] Ekre et al.[24] This article can be considered a generalization of the previous work, and, in particular, includes the following novelties: the model problem is a coupled two-field problem; the estimator (and the reduced model) are derived for a POD basis (in contrast to a SD basis); the implicit relation between $\boldsymbol{u}$ and p given by static equilibrium is utilized to (i) reduce the error equation to a one-field problem, and (ii) to construct the symmetric norm-inducing form.

4.2 | The error equation and corresponding residual

From linearity of $A_\square(\bullet, \bullet)$ we may establish the error equation: Find $g \in \mathcal{P}_\square$ such that

$$A_\square(g, q) = L_\square(q) - A_\square(p_R, q) =: R_\square(q) \quad \forall q \in \mathcal{Q}_\square, \tag{54}$$

where the residual is defined by

$$
\begin{aligned}
R_\square(q) &:= \int_I [\mathfrak{b}_\square(q, -\dot{\boldsymbol{u}}_{\bar{\varepsilon}} - \boldsymbol{u}_p^\mu\{\dot{p}_R\}) - m_\square(\dot{p}_{,R} q) - \mathfrak{a}_\square^{(p)}(p_R, q)] dt \\
&\quad + [m_\square(p_0 - p_R, q) + \mathfrak{b}_\square(q, \boldsymbol{u}_0 - \boldsymbol{u}_{\bar{\varepsilon}} - \boldsymbol{u}_p^\mu\{p_R\})]|_{t=0} \\
&= \int_I [m_\square(M_t, q)] dt + [m_\square(M_0, q)]|_{t=0}. \tag{55}
\end{aligned}
$$

In the last step, we collected all terms by defining M_t and M_0 from the following identities

$$M_t \in \mathbb{P}_\square: \quad m_\square(M_t, \delta p) = \mathfrak{b}_\square(\delta p, -\dot{\boldsymbol{u}}_{\bar{\varepsilon}} - \boldsymbol{u}_p^\mu\{\dot{p}_R\}) - m_\square(\dot{p}_R, \delta p) - \mathfrak{a}_\square^{(p)}(p_R, \delta p) \quad \forall \delta p \in \mathbb{P}_\square, \tag{56a}$$

$$M_0 \in \mathbb{P}_\square : \quad \mathfrak{m}_\square(M_0, \delta p) = \mathfrak{m}_\square(p_0 - p_R, \delta p) + \mathfrak{b}_\square\big(\delta p, \boldsymbol{u}_0 - \boldsymbol{u}_{\bar{\varepsilon}} - \boldsymbol{u}_p^\mu\{p_R\}\big) \quad \forall \delta p \in \mathbb{P}_\square. \tag{56b}$$

Remark 7. It is important to note that it is not necessary to solve M_t explicitly in each time step, since it is enough to compute the sensitivities w.r.t the time-dependent functions. The total computational effort for the error estimate is discussed further in Section 4.5. □

Since we are only concerned with the error stemming from the reduced basis, and hence consider (38) to be solved exactly, we note that

$$R_\square(q_R) = 0 \qquad \forall q_R \in \mathcal{Q}_{\square,R}, \tag{57}$$

and hence obtain the following, Galerkin-like, identity

$$R_\square(q) = R_\square(q) - R_\square(\Pi_R q) = R_\square(\Pi_C q) = \int_I [\mathfrak{m}_\square(\Pi_C M_t, q)]\mathrm{d}t + [\mathfrak{m}_\square(\Pi_C M_0, q)]|_{t=0} \qquad \forall q \in \mathcal{Q}_\square, \tag{58}$$

where we in the last step used the projection property from Equation (51).

4.3 | Auxiliary error equation and associated norm

In order to obtain a norm, and to construct an auxiliary problem where we avoid computation of the implicit relation $\boldsymbol{u}_p\{q\}$ for any $q \in \mathcal{P}_\square$, we introduce the auxiliary bilinear form $\hat{A}_\square(\bullet, \bullet)$, defined as follows

$$\hat{A}_\square(q, r) := \int_I \mathfrak{a}_\square^{(p)}(q, r)\mathrm{d}t + \frac{1}{2}\mathfrak{m}_\square(q, r)|_{t=0} + \frac{1}{2}\mathfrak{m}_\square(q, r)|_{t=T}, \tag{59}$$

cf. a similar approach in Parés et al.[27] We note that $\hat{A}_\square(\bullet, \bullet)$ defines a scalar product on the set

$$\hat{\mathcal{P}}_\square := \big\{q(\boldsymbol{x}, t) : q|_{t=0} \in \mathbb{P}_\square, \ q|_I \in L_2(I; \mathbb{P}_\square), \ q|_{t=T} \in \mathbb{P}_\square\big\}, \tag{60}$$

and hence it can be used to define a norm

$$\|q\| := \sqrt{\hat{A}_\square(q, q)}. \tag{61}$$

Furthermore, we note that[3] $\mathcal{P}_\square \subset \hat{\mathcal{P}}_\square$, and that any functional on $\mathcal{Q}_\square$ can be evaluated for functions in $\hat{\mathcal{P}}_\square$. Finally, for any function $q \in \mathcal{P}_\square$, we derive the following inequality

$$A_\square(q, q) = \int_I \left[\underbrace{\mathfrak{m}_\square(\dot{,} q)}_{\frac{1}{2}\frac{\mathrm{d}}{\mathrm{d}t}[\mathfrak{m}_\square(q,q)]} + \underbrace{\mathfrak{b}_\square(q, \boldsymbol{u}_p^\mu\{\})}_{\overset{(28)}{=}\mathfrak{a}_\square^{(u)}(\boldsymbol{u}_p^\mu\{q\}, \boldsymbol{u}_p^\mu\{\dot{q}\})} + \mathfrak{a}_\square^{(p)}(q, q) \right]\mathrm{d}t + \left[\mathfrak{m}_\square(q, q) + \underbrace{\mathfrak{b}_\square(q, \boldsymbol{u}_p^\mu\{q\})}_{\overset{(28)}{=}\mathfrak{a}_\square^{(u)}(\boldsymbol{u}_p^\mu\{q\}, \boldsymbol{u}_p^\mu\{q\})} \right]\Big|_{t=0}$$

$$= \int_I \left[\frac{1}{2}\frac{\mathrm{d}}{\mathrm{d}t}[\mathfrak{m}_\square(q, q)] + \underbrace{\mathfrak{a}_\square^{(u)}(\boldsymbol{u}_p^\mu\{q\}, \boldsymbol{u}_p^\mu\{\})}_{\frac{1}{2}\frac{\mathrm{d}}{\mathrm{d}t}\mathfrak{a}_\square^{(u)}(\boldsymbol{u}_p^\mu\{q\}, \boldsymbol{u}_p^\mu\{q\})} + \mathfrak{a}_\square^{(p)}(q, q) \right]\mathrm{d}t + \left[\mathfrak{m}_\square(q, q) + \mathfrak{a}_\square^{(u)}(\boldsymbol{u}_p^\mu\{q\}, \boldsymbol{u}_p^\mu\{q\}) \right]\Big|_{t=0}$$

$$= \int_I \left[\frac{1}{2}\frac{\mathrm{d}}{\mathrm{d}t}[\mathfrak{m}_\square(q, q)] + \frac{1}{2}\frac{\mathrm{d}}{\mathrm{d}t}[\mathfrak{a}_\square^{(u)}(\boldsymbol{u}_p^\mu\{q\}, \boldsymbol{u}_p^\mu\{q\})] + \mathfrak{a}_\square^{(p)}(q, q) \right]\mathrm{d}t + \left[\mathfrak{m}_\square(q, q) + \mathfrak{a}_\square^{(u)}(\boldsymbol{u}_p^\mu\{q\}, \boldsymbol{u}_p^\mu\{q\}) \right]\Big|_{t=0}$$

$$= \int_I \mathfrak{a}_\square^{(p)}(q, q)\mathrm{d}t + \frac{1}{2}[\mathfrak{m}_\square(q, q)]_{t=0}^{t=T} + \frac{1}{2}[\mathfrak{a}_\square^{(u)}(\boldsymbol{u}_p^\mu\{q\}, \boldsymbol{u}_p^\mu\{q\})]_{t=0}^{t=T} + \left[\mathfrak{m}_\square(q, q) + \mathfrak{a}_\square^{(u)}(\boldsymbol{u}_p^\mu\{q\}, \boldsymbol{u}_p^\mu\{q\}) \right]\Big|_{t=0}$$

---

[3]Recall the notation that $p(0)$ and $p(T)$ are included in $\mathcal{P}_\square$.

$$
= \int_I \mathfrak{a}_\square^{(p)}(q,q)\mathrm{d}t + \frac{1}{2}\underbrace{\mathfrak{m}_\square(q(0),q(0))}_{} + \frac{1}{2}\mathfrak{m}_\square(q(T),q(T)) + \underbrace{\frac{1}{2}\mathfrak{a}_\square^{(u)}(\boldsymbol{u}_P^\mu\{q(0)\},\boldsymbol{u}_P^\mu\{q(0)\})}_{\geq 0} + \underbrace{\frac{1}{2}\mathfrak{a}_\square^{(u)}(\boldsymbol{u}_P^\mu\{q(T)\},\boldsymbol{u}_P^\mu\{q(T)\})}_{\geq 0}
$$

$$
\underbrace{\phantom{\int_I \mathfrak{a}_\square^{(p)}(q,q)\mathrm{d}t + \frac{1}{2}\mathfrak{m}_\square(q(0),q(0)) + \frac{1}{2}\mathfrak{m}_\square(q(T),q(T))}}_{\hat{A}_\square(q,q)}
$$

$$
\geq \hat{A}_\square(q,q), \tag{62}
$$

i.e. the auxiliary form bounds $A_\square(\bullet,\bullet)$ from below.

We may now express an auxiliary error equation based on the form in Equation (59). Find $\hat{g} \in \hat{\mathcal{P}}_\square$ such that

$$
\hat{A}_\square(\hat{g},q) = R_\square(q) \qquad \forall q \in \hat{\mathcal{P}}_\square. \tag{63}
$$

The norm of the auxiliary error $\hat{g}$ provides an upper bound of the norm of the true error g

$$
\|g\| \leq \|\hat{g}\|, \tag{64}
$$

which follows from the inequality in (62), the definitions of the error equations in (54) and (63), and from using Cauchy-Schwartz inequality, i.e.

$$
\|g\|^2 = \hat{A}_\square(g,g) \overset{(62)}{\leq} A_\square(g,g) \overset{(54)}{=} R_\square(g) \overset{(63)}{=} \hat{A}_\square(\hat{g},g) \overset{\text{C–S}}{\leq} \|\hat{g}\|\|g\|. \tag{65}
$$

4.4 | Explicit NMR-error estimates

In what follows, we aim to derive an explicit upper estimate for $\|\hat{g}\|$, which will thus also serve as an upper bound of $\|g\|$. From the definition of the norm in (61), we obtain

$$
\|\hat{g}\| := \sqrt{\hat{A}_\square(\hat{g},\hat{g})} = \sqrt{\int_I \|\hat{g}\|_\mathfrak{a}^2 \mathrm{d}t + \frac{1}{2}\|\hat{g}\|_\mathfrak{m}^2|_{t=0} + \frac{1}{2}\|\hat{g}\|_\mathfrak{m}^2|_{t=T}}. \tag{66}
$$

We first note that, from the definition of the auxiliary form $\hat{A}_\square(\bullet,\bullet)$, the auxiliary error equation (63) localizes in time and can be expressed explicitly $t=0$, $t \in I$ and $t=T$. In the following three sections (4.4.1, 4.4.2, and 4.4.3) we consider (63) separately for these three cases and aim for explicit estimates for the three RVE-norms $\|\hat{g}\|_\mathfrak{m}|_{t=0}$, $\|\hat{g}\|_\mathfrak{a}|_{t\in I}$ and $\|\hat{g}\|_\mathfrak{m}|_{t=T}$ in (66), respectively. The final estimate of $\|\hat{g}\|$ is given in Section 4.4.4.

4.4.1 | Auxiliary error equation at time $t=0$

At time $t=0$ the auxiliary error equation (63) reduces to the problem of finding $\hat{g}(0) =: \hat{g}_0 \in \mathbb{P}_\square$ such that

$$
\frac{1}{2}\mathfrak{m}_\square(\hat{g}_0,q) = \mathfrak{m}_\square(\Pi_C M_0, q) \qquad \forall q \in \mathbb{P}_\square. \tag{67}
$$

With Cauchy-Schwarz inequality we obtain the following upper bound from (67):

$$
\|\hat{g}_0\|_\mathfrak{m}^2 = \mathfrak{m}_\square(\hat{g}_0,\hat{g}_0) \overset{(67)}{=} 2\mathfrak{m}_\square(\Pi_C M_0, \hat{g}_0) \overset{\text{C–S}}{\leq} 2\|\Pi_C M_0\|_\mathfrak{m}\|\hat{g}_0\|_\mathfrak{m}, \tag{68}
$$

and, thus, obtain an estimate for the contribution to $\|\hat{g}\|$ at $t=0$

$$
\frac{1}{2}\|\hat{g}(0)\|_\mathfrak{m}^2 \leq 2\|\Pi_C M_0\|_\mathfrak{m}^2. \tag{69}
$$

4.4.2 | Auxiliary error equation at time $t \in I$

In the time interval the auxiliary error equation (63) reduces to the problem of finding $\hat{g}(t) =: \; \hat{g}_t \in \mathbb{P}_\square$ such that

$$\mathfrak{a}_\square^{(p)}(\hat{g}_t, q) = \mathfrak{m}_\square(\Pi_C M_t, q) \qquad \forall q \in \mathbb{P}_\square, \tag{70}$$

and we obtain the following upper bound using Cauchy-Schwartz inequality

$$\|\hat{g}_t\|_\mathfrak{a}^2 = \mathfrak{a}_\square^{(p)}(\hat{g}_t, \hat{g}_t) = \mathfrak{m}_\square(\Pi_C M_t, \hat{g}_t) \overset{C-S}{\leq} \|\Pi_C M_t\|_\mathfrak{m} \|\hat{g}_t\|_\mathfrak{m}. \tag{71}$$

To proceed we need a relation between $\|\hat{g}_t\|_\mathfrak{m}$ and $\|\hat{g}_t\|_\mathfrak{a}$. To this end, we use SD and write $\hat{g}_t = \sum_{a=1}^N \varphi_a \xi_a$ where ξ_a are coefficients to the corresponding eigenmodes φ_a from the solution of the eigenvalue problem

$$\mathfrak{a}_\square^{(p)}(\varphi_a, \delta p) = \lambda_a \mathfrak{m}_\square(\varphi_a, \delta p) \quad \forall \delta p \in \mathbb{P}_\square \qquad\qquad a = 1, 2, \ldots, N, \tag{72a}$$

$$\mathfrak{m}_\square(\varphi_a, \varphi_b) = \delta_{ab} \qquad\qquad a, b = 1, 2, \ldots, N, \tag{72b}$$

with eigenvalues λ_a sorted in increasing order, such that $\lambda_1 \leq \lambda_2, \ldots$. With $\hat{g}_t$ written as the spectral expansion we can obtain the following inequality

$$\|\hat{g}_t\|_\mathfrak{m}^2 = \|\sum_{a=1}^N \varphi_a \xi_a\|_\mathfrak{m}^2 = \sum_{a=1}^N \xi_a^2 = \frac{1}{\lambda_{min}} \sum_{a=1}^N \lambda_{min} \xi_a^2 \leq \frac{1}{\lambda_{min}} \sum_{a=1}^N \lambda_a \xi_a^2 = \frac{1}{\lambda_{min}} \|\sum_{a=1}^N \varphi_a \xi_a\|_\mathfrak{a}^2 = \frac{1}{\lambda_{min}} \|\hat{g}_t\|_\mathfrak{a}^2. \tag{73}$$

Finally, with (71) and (73), we arrive at the following upper bound for the time interval contribution to $\|\hat{g}\|$

$$\|\hat{g}(t)\|_\mathfrak{a}^2 \leq \frac{\|\Pi_C M_t\|_\mathfrak{m}^2}{\lambda_{min}}. \tag{74}$$

Remark 8. We note that the eigenvalue problem in (72) is equivalent to the eigenvalue problem from Section 3.4.2, where it was used to identify a spectral base for the reduced field. Thus, if such a base is used for the reduction, we may use the same strategy as in Aggestam et al[23] and exchange λ_{min} to λ_{N_R}, resulting in a sharper bound. $\qquad\square$

4.4.3 | Auxiliary error equation at time $t = T$

At time $t = T$ the auxiliary error equation reduces to the problem of finding $\hat{q}(T) =: \; \hat{q}_T \in \mathbb{P}_\square$ such that

$$\frac{1}{2} \mathfrak{m}_\square(\hat{g}_T, q) = 0 \qquad \forall q \in \mathbb{P}_\square, \tag{75}$$

and, since $\mathfrak{m}_\square(\bullet, \bullet)$ is coercive, this leads to the trivial result

$$\frac{1}{2} \|\hat{g}(T)\|_\mathfrak{m}^2 \equiv 0. \tag{76}$$

4.4.4 | Final estimate of the energy norm

Equation (66) together with estimates given in (69), (74) and (76) now gives the final error estimate in the energy norm

$$\|\hat{g}\| = \sqrt{\int_I \|\hat{g}\|_\mathfrak{a}^2 \mathrm{d}t + \frac{1}{2} \|\hat{g}\|_\mathfrak{m}^2 |_{t=0} + \frac{1}{2} \|\hat{g}\|_\mathfrak{m}^2 |_{t=T}} \leq \sqrt{\int_I \frac{\|\Pi_C M_t\|_\mathfrak{m}^2}{\lambda_{min}} \mathrm{d}t + 2\|\Pi_C M_0\|_\mathfrak{m}^2} =: \; E_{est}. \tag{77}$$

The estimate is similar to the estimate given for the transient heat flow problem in Equation (112) from Aggestam et al,[23] with some important differences:

- in Aggestam et al[23] the norm inducing functional is equal to the original functional for the same argument[4], whereas here, in Equation (65), we need an extra inequality, $\|g\|^2 = \hat{A}_\square(g,g) \leq A_\square(g,g)$, due to the handling of the term coupling the fields;
- in Aggestam et al[23] the eigenvalue in the estimate is chosen to the largest resolved eigenvalue, which is possible since a spectral based is used for the reduction, whereas here we need to use the lowest eigenvalue in the general case.[5]

4.5 | Quantification of computational effort for the estimate

The final estimate in Equation (77) requires the solution to the auxiliary problems for M_t and M_0 from Equation (56). As mentioned in Section 4.2 it is not necessary to solve for M_t in each time step, it is enough to solve for the sensitivities w.r.t the time-dependent quantities. For M_t it is sufficient to solve $6 + N_R$ linear static problems[6]; one for each macroscale strain component, and one for each mode in the reduced basis. For M_0 there is one extra solution for the initial condition. In particular it is important to note that the number of auxiliary solves is fixed and does not scale with neither mesh size nor the number of time steps. These $6 + N_R$ functions can be precomputed, and, when they are known, the estimate in (77) is fully explicit and efficient to evaluate.

5 | GOAL ORIENTED ESTIMATION OF THE NMR ERROR

5.1 | Preliminaries

In this section, we will discuss quantification of the error in terms of user-defined quantities of interest (QoI) using goal oriented error estimation. The procedure to obtain the explicit estimate follows the steps in Section 4 closely, and in particular, we will again only focus on the error introduced by the reduced base, and ignore space-time discretization errors by considering the fully resolved finite element problem to be the exact solution.

For the goal oriented error estimation, we use the following "building blocks":

- definition of linear output functional for the chosen quantity of interest (Section 5.2);
- definition of the dual problem and corresponding reduced dual problem (Section 5.3);
- formulation of the dual residual and the dual error with upper and lower bounds (Sections 5.4 and 5.5);
- construction of explicit error bounds for the error in the quantity of interest (Section 5.6).

5.2 | Linear output functional

We introduce linear goal functionals $Q_\square^{(u)}, Q_\square^{(p)}$, corresponding to the original (uncondensed) RVE problem in (22), that represents the Quantity of Interest (QoI)

$$Q_\square^{(u)}(\boldsymbol{u}) := \int_I [\mathfrak{q}_{\square,t}^{(u)}(t;\boldsymbol{u})]\mathrm{d}t + \mathfrak{q}_{\square,T}^{(u)}(\boldsymbol{u}(T)), \tag{78a}$$

$$Q_\square^{(p)}(p) := \int_I [\mathfrak{q}_{\square,t}^{(p)}(t;p)]\mathrm{d}t + \mathfrak{q}_{\square,T}^{(p)}(p(T)). \tag{78b}$$

---

[4]In particular, from Equation (74) in Aggestam et al[23] there is $\|e\|^2 = A_\square^s(e,e) = A_\square(e,e)$ for the error e.

[5]As mentioned in Section 3.4.2 it is possible to use a spectral base for problem discussed in this article, in which case the largest resolved eigenvalue can be used in the estimate, as noted in Section 4.4.2.

[6]The auxiliary problems are of size N, for example, the size of the underlying finite element problem that the reduced basis is based on, and have a "mass matrix" as the left-hand side.

For the condensed problem (32), we can clearly reformulate the QoI as

$$Q_\square(p) := Q_\square^{(u)}(\boldsymbol{u}_{\bar\varepsilon} + \boldsymbol{u}_p\{p\}) + Q_\square^{(p)}(p). \tag{79}$$

However, for the subsequent error analysis we wish to establish $\boldsymbol{u}_p\{\bullet\}$ for the entire $\mathbb{P}_\square$, and not just for $\mathbb{P}_{\square,\mathrm{R}}$ as was done in Subsection 3.2. To this end, we establish the following problems to solve for auxiliary "influence functions" $\boldsymbol{u}_t^\star(t) \in \mathbb{U}_\square^0$ and $\boldsymbol{u}_T^\star \in \mathbb{U}_\square^0$:

$$\mathfrak{a}_\square^{(u)}(\delta\boldsymbol{u}, \boldsymbol{u}_t^\star(t)) = \mathfrak{q}_{\square,t}^{(u)}(t; \delta\boldsymbol{u}) \quad \forall \delta\boldsymbol{u} \in \mathbb{U}_\square^0, \; \forall t \in I, \tag{80a}$$

$$\mathfrak{a}_\square^{(u)}(\delta\boldsymbol{u}, \boldsymbol{u}_T^\star) = \mathfrak{q}_{\square,T}^{(u)}(\delta\boldsymbol{u}) \quad \forall \delta\boldsymbol{u} \in \mathbb{U}_\square^0. \tag{80b}$$

We may now rewrite (79) as an explicit expression in p, by using the auxiliary dual problems in (80), and the definition of the implicit function $\boldsymbol{u}_p$ in (28)

$$Q_\square(p) = \int_I [\mathfrak{q}_{\square,t}^{(u)}(t; \boldsymbol{u}_{\bar\varepsilon}) + \mathfrak{q}_{\square,t}^{(u)}(t; \boldsymbol{u}_p\{p\}) + \mathfrak{q}_{\square,t}^{(p)}(t; p)]\mathrm{d}t + \mathfrak{q}_{\square,T}^{(u)}(\boldsymbol{u}_0(T)) + \mathfrak{q}_{\square,T}^{(u)}(\boldsymbol{u}_p\{p(T)\}) + \mathfrak{q}_{\square,T}^{(p)}(p(T))$$

$$\overset{(80)}{=} \int_I [\mathfrak{q}_{\square,t}^{(u)}(t; \boldsymbol{u}_{\bar\varepsilon}) + \mathfrak{a}_\square^{(u)}(\boldsymbol{u}_p\{p\}, \boldsymbol{u}_t^\star) + \mathfrak{q}_{\square,T}^{(p)}(t; p)]\mathrm{d}t + \mathfrak{q}_{\square,t}^{(u)}(\boldsymbol{u}_0(T)) + \mathfrak{a}_\square^{(u)}(\boldsymbol{u}_p\{p(T)\}, \boldsymbol{u}_T^\star) + \mathfrak{q}_{\square,T}^{(p)}(p(T))$$

$$\overset{(28)}{=} \int_I [\mathfrak{q}_{\square,t}^{(u)}(t; \boldsymbol{u}_{\bar\varepsilon}) + \mathfrak{b}_\square(p, \boldsymbol{u}_t^\star) + \mathfrak{q}_{\square,t}^{(p)}(t; p)]\mathrm{d}t + \mathfrak{q}_{\square,T}^{(u)}(\boldsymbol{u}_0(T)) + \mathfrak{b}_\square(p(T), \boldsymbol{u}_T^\star) + \mathfrak{q}_{\square,T}^{(p)}(p(T)). \tag{81}$$

Equation (81) now represents the output and is fully explicit in p. Finally, we may express the functional for the error $g = p - p_{\mathrm{R}}$

$$\overline{Q}_\square(g) := Q_\square(p) - Q_\square(p_{\mathrm{R}}) = \int_I [\mathfrak{b}_\square(g, \boldsymbol{u}_t^\star) + \mathfrak{q}_{\square,t}^{(p)}(t; g)]\mathrm{d}t + \mathfrak{b}_\square(g(T), \boldsymbol{u}_T^\star) + \mathfrak{q}_{\square,T}^{(p)}(g(T)), \tag{82}$$

which is an explicit functional on the space

$$\mathcal{Q}_\square^\star = \{q(\boldsymbol{x}, t) : \; q|_I \in L_2(I; \mathbb{P}_\square), \; q|_{t=T} \in \mathbb{P}_\square\}. \tag{83}$$

Example: Time-averaged homogenized stress

Consider the ij-component of the homogenized stress, $\overline\sigma_{ij}$, as the Quantity of Interest. The output functional can thus be defined by

$$\mathfrak{q}_{\square,t}^{(u)}(t; \boldsymbol{u}) = \frac{1}{|I||\Omega_\square|} \int_{\Omega_\square} [\boldsymbol{e}_i \otimes \boldsymbol{e}_j \; : \; \mathbf{E}:\varepsilon[\boldsymbol{u}]]\mathrm{d}\Omega, \tag{84a}$$

$$\mathfrak{q}_{\square,T}^{(u)}(\boldsymbol{u}) = 0, \tag{84b}$$

$$\mathfrak{q}_{\square,t}^{(p)}(t; p) = \frac{1}{|I||\Omega_\square|} \int_{\Omega_\square} [-\alpha p \delta_{ij}]\mathrm{d}\Omega, \tag{84c}$$

$$\mathfrak{q}_{\square,T}^{(p)}(p) = 0. \tag{84d}$$

We note, in particular, that this functional does not depend on time, and therefore it is enough to solve the auxiliary problems (80a) *once*, instead of *once per time step*, which is needed in the general case.

5.3 | Dual problem

We define the dual problem as that of finding $p^\star \in \mathcal{P}_\square$ such that

$$A_\square^\star(p^\star, q) = \overline{Q}_\square(q) \quad \forall q \in Q_\square^\star, \tag{85}$$

where we recall the test space $Q_\square^\star$ from (83), and where the dual form $A_\square^\star$ is defined as

$$A_\square^\star(q, r) := \int_I [-\mathfrak{m}_\square(\dot{q}, r) - \mathfrak{b}_\square(r, \boldsymbol{u}_p\{\dot{q}\}) + \mathfrak{a}_\square^{(p)}(q, r)] \mathrm{d}t + \mathfrak{m}_\square(q(T), r(T)) + \mathfrak{b}_\square(r(T), \boldsymbol{u}_p\{q(T)\}). \tag{86}$$

We note that, for $q, r \in \mathcal{P}_\square$

$$A_\square(q, r) = A_\square^\star(r, q), \tag{87}$$

which follows from integration by parts, namely,

$$\int_I \mathfrak{m}_\square(\dot{q}, r) \mathrm{d}t + \mathfrak{m}_\square(q(0), r(0)) = \int_I \left[\frac{\mathrm{d}}{\mathrm{d}t}[\mathfrak{m}_\square(q, r)] - \mathfrak{m}_\square(q, \dot{r}) \right] \mathrm{d}t + \mathfrak{m}_\square(q(0), r(0))$$

$$= \int_I - \mathfrak{m}_\square(q, \dot{r}) + [\mathfrak{m}_\square(q, r)]_0^T + \mathfrak{m}_\square(q(0), r(0)) = \int_I - \mathfrak{m}_\square(\dot{r}, q) \mathrm{d}t + \mathfrak{m}_\square(r(T), q(T)), \tag{88}$$

and

$$\int_I \mathfrak{b}_\square(r, \boldsymbol{u}_p\{\dot{q}\}) \mathrm{d}t + \mathfrak{b}_\square(r(0), \boldsymbol{u}_p\{q(0)\}) \stackrel{(28)}{=} \int_I \mathfrak{a}_\square^{(u)}(\boldsymbol{u}_p\{r\}, \boldsymbol{u}_p\{\dot{q}\}) \mathrm{d}t + \mathfrak{b}_\square(q(0), \boldsymbol{u}_p\{r(0)\})$$

$$\int_I \left[\frac{\mathrm{d}}{\mathrm{d}t}[\mathfrak{a}_\square^{(u)}(\boldsymbol{u}_p\{r\}, \boldsymbol{u}_p\{q\})] - \mathfrak{a}_\square^{(u)}(\boldsymbol{u}_p\{\dot{r}\}, \boldsymbol{u}_p\{q\}) \right] \mathrm{d}t + \mathfrak{b}_\square(q(0), \boldsymbol{u}_p\{r(0)\})$$

$$\stackrel{(28)}{=} \int_I [-\mathfrak{b}_\square(q, \boldsymbol{u}_p\{\dot{r}\})] \mathrm{d}t + [\mathfrak{b}_\square(q, \boldsymbol{u}_p\{r\})]_0^T + \mathfrak{b}_\square(q(0), \boldsymbol{u}_p\{r(0)\})$$

$$= \int_I [-\mathfrak{b}_\square(q, \boldsymbol{u}_p\{\dot{r}\})] \mathrm{d}t + \mathfrak{b}_\square(q(T), \boldsymbol{u}_p\{r(T)\}). \tag{89}$$

The **reduced dual problem** is defined as that of finding $p_R^\star \in \mathcal{P}_{\square,R}$ such that

$$A_\square^\star(p_R^\star, q_R) = \overline{Q}_\square(q_R) \quad \forall q_R \in Q_{\square,R}^\star, \tag{90}$$

where $Q_{\square,R}^\star$ follows from (83), with $\mathbb{P}_\square$ replaced with $\mathbb{P}_{\square,R}$.

5.4 | Dual error equation and corresponding residual

We define the dual error equation as the problem of finding $g^\star \in \mathcal{P}_\square$ such that

$$A_\square^\star(g^\star, q) = \overline{Q}_\square(q) - A_\square^\star(p_R^\star, q) =: R_\square^\star(q) \quad \forall q \in Q_\square^\star \tag{91}$$

where $g^\star := p^\star - p_R^\star$ is the error in the dual solution. Consequently, due to (87) and the Galerkin orthogonality in (54) we obtain

$$A_\square^\star(g^\star, g) = \overline{Q}_\square(g) - A_\square^\star(p_R^\star, g) = \overline{Q}_\square(g) - A_\square(g, p_R^\star) = \overline{Q}_\square(g), \tag{92}$$

since $p_R^\star \in \mathcal{P}_{\square,R} \subset Q_{\square,R}$.

The dual residual is expanded similar to Subsection 4.2

$$R_\square^\star(q) = \int_I [\mathfrak{b}_\square(q, \boldsymbol{u}_t^\star) + \mathfrak{q}_{\square,t}^{(p)}(t; q) + \mathfrak{m}_\square(\dot{p}_R^\star, q) + \mathfrak{b}_\square(q, \boldsymbol{u}_p\{\dot{p}_R^\star\}) - \mathfrak{a}_\square^{(p)}(p_R^\star, q)] \mathrm{d}t$$

$$+ \mathfrak{b}_\square(q(T), \boldsymbol{u}_T^\star) + \mathfrak{q}_{\square,T}^{(p)}(q(T)) - \mathfrak{m}_\square(p_R^\star(T), q(T)) - \mathfrak{b}_\square(q(T), \boldsymbol{u}_p\{p_R^\star(T)\})$$

$$= \int_I \mathfrak{m}_\square(M_t^\star, q) \mathrm{d}t + \mathfrak{m}_\square(M_T^\star, q(T)) \tag{93}$$

In the last step we, once again, collected all the terms by defining $M_t^\star$ and $M_T^\star$ from the following identities

$$M_t^\star \in \mathbb{P}_\square : \quad \mathfrak{m}_\square(M_t^\star, \delta p) = \mathfrak{b}_\square(\delta p, \boldsymbol{u}_t^\star + \boldsymbol{u}_p\{\dot{p}_R^\star\}) + \mathfrak{q}_{\square,t}^{(p)}(t; \delta p) + \mathfrak{m}_\square(\dot{p}_R^\star, \delta p) - \mathfrak{a}_\square^{(p)}(p_R^\star, \delta p) \quad \forall \delta p \in \mathbb{P}_\square, \tag{94a}$$

$$M_T^\star \in \mathbb{P}_\square : \quad \mathfrak{m}_\square(M_T^\star, \delta p) = \mathfrak{b}_\square(\delta p, \boldsymbol{u}_T^\star - \boldsymbol{u}_p\{p_R^\star(T)\}) + \mathfrak{q}_{\square,T}^{(p)}(\delta p) - \mathfrak{m}_\square(p_R^\star(T), \delta p) \quad \forall \delta p \in \mathbb{P}_\square. \tag{94b}$$

Remark 9. We once again note that it is not necessary to solve for $M_t^\star$ explicitly in each time step, it is enough to solve for the sensitivities w.r.t. the time-dependent functions. The total computational effort for the error estimate is discussed further in Section 5.7. □

As with the energy norm error estimate in Section 4.2, we are only concerned with the error stemming from the reduced basis, and hence consider (90) to be solved exactly. For the residual this means that

$$R_\square^\star(q_R) = 0 \quad \forall q_R \in Q_{\square,R}^\star, \tag{95}$$

and we, once again, obtain the following, Galerkin-like, identity

$$R_\square^\star(q) = R_\square^\star(q) - R_\square^\star(\Pi_R q) = R_\square^\star(\Pi_C q) = \int_I [\mathfrak{m}_\square(\Pi_C M_t^\star, q)] dt + [\mathfrak{m}_\square(\Pi_C M_T^\star, q)]|_{t=T} \quad \forall q \in Q_\square^\star, \tag{96}$$

where we, in the last step, used the projection property from Equation (51).

5.5 | Dual error estimate—Upper and lower bounds

To find an estimate for the defined quantity of interest we first define the auxiliary dual error equation using the auxiliary form (59) from Subsection 4.3; Find $\hat{g}^\star \in \hat{\mathcal{P}}_\square$ such that

$$\hat{A}_\square(\hat{g}^\star, q) = R_\square^\star(q) \quad \forall q \in \hat{\mathcal{P}}_\square. \tag{97}$$

Remark 10. With the same argumentation as in Subsection 4.4, the solution $\hat{g}^\star$ provides an upper bound of the exact dual error as follows:

$$\|g^\star\| \leq \|\hat{g}^\star\|, \tag{98}$$

since

$$\|g^\star\|^2 = \hat{A}_\square(g^\star, g^\star) \leq A_\square^\star(g^\star, g^\star) = R_\square^\star(g^\star) = \hat{A}_\square(\hat{g}^\star, g^\star) \leq \|\hat{g}^\star\|\|g^\star\|. \tag{99}$$

□

In addition to the auxiliary dual error equation, we also introduce the "composite errors," $g^\pm$ and $\hat{g}^\pm$, as linear combinations of the corresponding primal and dual parts, viz.

$$g^\pm := \kappa g \pm \frac{1}{\kappa} g^\star \quad \in \mathcal{P}_\square, \tag{100a}$$

$$\hat{g}^\pm := \kappa \hat{g} \pm \frac{1}{\kappa} \hat{g}^\star \quad \in \hat{\mathcal{P}}_\square, \tag{100b}$$

for any $\kappa \neq 0$. Due to linearity, the auxiliary composite error $\hat{g}^\pm$ is the solution to

$$\hat{A}_\square(\hat{g}^\pm, q) = \kappa R_\square(q) \pm \frac{1}{\kappa} R_\square^\star(q) =: R_\square^\pm(q) \quad \forall q \in \hat{\mathcal{P}}_\square, \tag{101}$$

with the combined residual $R_\square^\pm$ defined explicitly as

$$R_\square^\pm(q) = \int_I \mathfrak{m}_\square(\Pi_C M_t^\pm, q) dt + [\mathfrak{m}_\square(\Pi_C M_0^\pm, q)]|_{t=0} + [\mathfrak{m}_\square(\Pi_C M_T^\pm, q)]|_{t=T}, \tag{102}$$

where we introduced

$$M_0^\pm := \kappa M_0, \tag{103a}$$

$$M_t^\pm := \kappa M_t \pm \frac{1}{\kappa} M_t^\star, \tag{103b}$$

$$M_T^\pm := \pm \frac{1}{\kappa} M_T^\star. \tag{103c}$$

Consider now the following equalities[7]:

$$\hat{A}_\square(\hat{g}^\pm, g^\pm) = \kappa^2 \hat{A}_\square(\hat{g}, g) \pm [\hat{A}_\square(\hat{g}, g^\star) + \hat{A}_\square(\hat{g}^\star, g)] + \kappa^{-2} \hat{A}_\square(\hat{g}^\star, g^\star) =$$
$$= \pm 2\overline{Q}_\square(g) + \kappa^2 \hat{A}_\square(\hat{g}, g) + \kappa^{-2} \hat{A}_\square(\hat{g}^\star, g^\star), \tag{104}$$

where we in the last step used the following identities, derived from the error equations and the Galerkin orthogonality

$$\hat{A}_\square(\hat{g}, g^\star) \overset{(63)}{=} R_\square(g^\star) \overset{(54)}{=} A_\square(g, g^\star) \overset{(87)}{=} A_\square^\star(g^\star, g) \overset{(92)}{=} \overline{Q}_\square(g), \tag{105a}$$

$$\hat{A}_\square(\hat{g}^\star, g) \overset{(97)}{=} R_\square^\star(g) \overset{(91)}{=} A_\square^\star(g^\star, g) \overset{(92)}{=} \overline{Q}_\square(g). \tag{105b}$$

In a procedure resembling the Parallelogram law, cf. Oden and Prudhomme,[29] we subtract the "−"-equation from the "+"-equation in (104) and obtain

$$\overline{Q}_\square(g) = \frac{1}{4}[\hat{A}_\square(\hat{g}^+, g^+) - \hat{A}_\square(\hat{g}^-, g^-)], \tag{106}$$

where the terms in the right-hand side of (106) can be bounded from below,

$$\hat{A}_\square(\hat{g}^\pm, g^\pm) = R_\square^\pm(g^\pm) = A_\square(g^\pm, g^\pm) \geq \|g^\pm\|^2, \tag{107}$$

and from above using Cauchy-Schwartz inequality,

$$\hat{A}_\square(\hat{g}^\pm, g^\pm) \leq \|\hat{g}^\pm\| \|g^\pm\|. \tag{108}$$

We can now obtain upper and lower bounds on $\overline{Q}_\square(g)$ by combining (106) with (107) and (108)

$$\frac{1}{4}[\|g^+\|^2 - \|\hat{g}^-\| \|g^-\|] \leq \overline{Q}_\square(g) \leq \frac{1}{4}[\|\hat{g}^+\| \|g^+\| - \|g^-\|^2]. \tag{109}$$

In what follows we will use the trivial lower bound, $\|g^\pm\| \geq 0$. Utilizing a sharper lower bound for $\|g^\pm\|$ would naturally result in a sharper estimate. However, it requires implicit procedures, which would make the final estimate more computational demanding. As a last step, we also utilize the bounds given by (65) and (98) and arrive at upper and lower bounds for the error in the quantity of interest

$$E_Q^- := -\frac{1}{4}\|\hat{g}^-\|^2 \leq \overline{Q}_\square(g) \leq \frac{1}{4}\|\hat{g}^+\|^2 =: E_Q^+. \tag{110}$$

5.6 | Explicit bounds for the error in quantity of interest

In order to obtain explicit upper and lower bounds for E_Q^- and E_Q^+ from Equation (110) we need an estimate for the norm of the composite error, $\|\hat{g}^\pm\|$. To this end, we use the strategy described in Subsection 4.4 and consider the composite error equation (101) localized in time for times $t = 0$, $t \in I$ and $t = T$ separately.

---

[7]Note that we here use the subscript $\pm$ as an alternative to presenting two equations; one "+" and one "−".

5.6.1 | Composite error equation at $t = 0$

At time $t = 0$ the composite error equation reduces to finding $\hat{g}^{\pm}(0) =: \ \hat{g}_0^{\pm} \in \mathbb{P}_{\square}$ such that

$$\frac{1}{2}\mathfrak{m}_{\square}(\hat{g}_0^{\pm}, q) = \mathfrak{m}_{\square}(\Pi_{\mathrm{C}} M_0^{\pm}, q) \quad \forall q \in \mathbb{P}_{\square}. \tag{111}$$

In terms of the norm, we obtain the following upper bound, using Cauchy-Schwartz inequality

$$\|\hat{g}_0^{\pm}\|_{\mathfrak{m}}^2 = \mathfrak{m}_{\square}(\hat{g}_0^{\pm}, \hat{g}_0^{\pm})|_{t=0} = 2\mathfrak{m}_{\square}(\Pi_{\mathrm{C}} M_0^{\pm}, \hat{g}_0^{\pm})|_{t=0} \leq 2\|\Pi_{\mathrm{C}} M_0^{\pm}\|_{\mathfrak{m}}\|\hat{g}_0^{\pm}\|_{\mathfrak{m}}, \tag{112}$$

and obtain the following contribution to $\|g^{\pm}\|$ at $t = 0$

$$\frac{1}{2}\|\hat{g}^{\pm}(0)\|_{\mathfrak{m}}^2 \leq 2\|\Pi_{\mathrm{C}} M_0^{\pm}\|_{\mathfrak{m}}^2. \tag{113}$$

5.6.2 | Composite error equation for $t \in I$

In the time interval, $t \in I$, the composite error equation reduces to finding $\hat{g}^{\pm}(t) =: \ \hat{g}_t^{\pm} \in \mathbb{P}_{\square}$ such that

$$\mathfrak{a}_{\square}^{(p)}(\hat{g}_t^{\pm}, q) = \mathfrak{m}_{\square}(\Pi_{\mathrm{C}} M_t^{\pm}, q) \quad \forall q \in \mathbb{P}_{\square}, \tag{114}$$

and, by using the same arguments as in Section 4.4.2, we obtain the following upper bound for the contribution to $\|\hat{g}^{\pm}\|$

$$\|\hat{g}^{\pm}(t)\|_{\mathfrak{a}}^2 \leq \frac{\|\Pi_{\mathrm{C}} M_t^{\pm}\|_{\mathfrak{m}}^2}{\lambda_{\min}}. \tag{115}$$

5.6.3 | Composite error equation for $t = T$

At time $t = T$ the composite error equation reduces to finding $\hat{g}^{\pm}(T) =: \ \hat{g}_T^{\pm} \in \mathbb{P}_{\square}$ such that

$$\frac{1}{2}\mathfrak{m}_{\square}(\hat{g}_T^{\pm}, q) = \mathfrak{m}_{\square}(M_T^{\pm}, q) \quad \forall q \in \mathbb{P}_{\square}, \tag{116}$$

and with the same arguments as in Section 5.6.1 we obtain the following upper bound of the contribution to $\|\hat{g}^{\pm}\|$

$$\frac{1}{2}\|\hat{g}^{\pm}(T)\|_{\mathfrak{m}}^2 \leq 2\|\Pi_{\mathrm{C}} M_T^{\pm}\|_{\mathfrak{m}}^2. \tag{117}$$

5.6.4 | Final upper and lower estimate for the error in quantity of interest

With the norm from Equation (66), the bounds from Equations (113), (115), and (117), and the upper and lower bounds of the Quantity of Interest from Equation (110) we obtain the following explicit estimates

$$E_{\mathrm{Q}}^+ \leq E_{\mathrm{Q,est}}^+ \ := \ \frac{1}{4}\min_{\kappa}\left[\int_I \frac{\|\Pi_{\mathrm{C}} M_t^+(\kappa)\|_{\mathfrak{m}}^2}{\lambda_{\min}}\mathrm{d}t + 2\|\Pi_{\mathrm{C}} M_0^+(\kappa)\|_{\mathfrak{m}}^2 + 2\|\Pi_{\mathrm{C}} M_T^+(\kappa)\|_{\mathfrak{m}}^2\right] \tag{118a}$$

$$E_{\mathrm{Q}}^- \geq E_{\mathrm{Q,est}}^- \ := \ -\frac{1}{4}\min_{\kappa}\left[\int_I \frac{\|\Pi_{\mathrm{C}} M_t^-(\kappa)\|_{\mathfrak{m}}^2}{\lambda_{\min}}\mathrm{d}t + 2\|\Pi_{\mathrm{C}} M_0^-(\kappa)\|_{\mathfrak{m}}^2 + 2\|\Pi_{\mathrm{C}} M_T^-(\kappa)\|_{\mathfrak{m}}^2\right] \tag{118b}$$

Finally, the estimates can be optimized by finding an optimal value of κ. We note that Equation (118) can be written as

$$E^+_{\text{Q,est}} = \frac{1}{4}\min_{\kappa}[A\kappa^2 + 2B + C\kappa^{-2}] \tag{119a}$$

$$E^-_{\text{Q,est}} = -\frac{1}{4}\min_{\kappa}[A\kappa^2 - 2B + C\kappa^{-2}] \tag{119b}$$

with coefficients

$$A := \int_I \frac{\|\Pi_C M_t\|^2_{\mathfrak{m}}}{\lambda_{\min}}dt + 2\|\Pi_C M_0\|^2_{\mathfrak{m}}, \tag{120a}$$

$$B := \int_I \frac{\mathfrak{m}_\square(\Pi_C M_t, \Pi_C M_t^\star)}{\lambda_{\min}}dt, \tag{120b}$$

$$C := \int_I \frac{\|\Pi_C M_t^\star\|^2_{\mathfrak{m}}}{\lambda_{\min}}dt + 2\|\Pi_C M_T^\star\|^2_{\mathfrak{m}}. \tag{120c}$$

Solving the trivial minimization problem, we obtain $\kappa^2_{\text{opt}} = \sqrt{\frac{C}{A}}$, which results in the following explicit upper and lower bounds

$$E^+_{\text{Q,est}} = \frac{1}{4}[\sqrt{AC} + 2B] \tag{121a}$$

$$E^-_{\text{Q,est}} = -\frac{1}{4}[\sqrt{AC} - 2B] \tag{121b}$$

5.7 | Quantification of computational effort for the estimate

Similar to the final estimate for the energy norm, the estimates in Equation (121) requires the solution to some auxiliary problems; Equation (80) for $\boldsymbol{u}_t^\star$ and $\boldsymbol{u}_T^\star$, Equation (94) for $M_t^\star$ and $M_T^\star$ and Equation (56) for M_t and M_0. For each quantity of interest, $\boldsymbol{u}_t^\star$ and $\boldsymbol{u}_T^\star$ requires one linear static solve each.[8]

Solving for $M_t^\star$ requires $6 + N_R$, and for $M_t^\star$ 1, linear static problem(s). Once again we emphasize that these are all computations that can be performed in the "offline" stage, stored, and then used for the error estimation throughout the "online" stage.

6 | NUMERICAL EXAMPLES

For the numerical examples we consider two different RVEs in three spatial dimensions. The RVEs consist of gas saturated matrix material (phase 1) with spherical, water saturated, inclusions of two different types (phases 2 and 3, respectively). The material parameters for the three phases are presented in Table 1.

In order to quantify the sharpness of the error estimate (as compared with the exact error) we define the effectivity index as

$$\eta := \frac{E_{\text{est}}}{E}, \tag{122}$$

where E_{est} is the estimate (Equation (77)), and E the exact error. Similarly, for the goal oriented estimate we define

$$\eta_Q := \frac{E_{\text{Q,est}}}{|E_Q|}, \qquad E_{\text{Q,est}} := \max(|E^+_{\text{Q,est}}|, |E^-_{\text{Q,est}}|), \tag{123}$$

---

[8]Assuming that the quantity of interest is independent of time, as the example in Section 5.2.

TABLE 1 Material parameters for the three material phases in the RVEs used for the numerical examples

		Phase 1 (matrix)	Phase 2 (inclusions)	Phase 3 (inclusions)
G	(GPa)	8.8	15.8	15.8
K	(GPa)	9.6	16.2	16.2
ϕ	(–)	0.2	0.1	0.1
K^{s}	(GPa)	36	36	36
K^{f}	(GPa)	0.022	2.3	2.3
k	(m² MPa⁻¹ s⁻¹)	2	0.033	0.0033

Abbreviation: RVEs, representative volume elements.
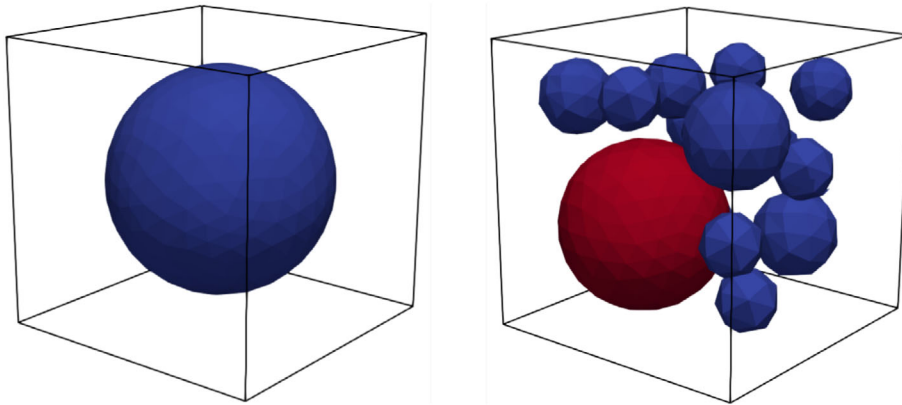
FIGURE 1 RVEs used for the numerical examples. To the left a single spherical inclusion of Phase 2 embedded in matrix of Phase 1 used for Example 1, and to the right multiple spherical inclusions of Phase 2 (blue) and Phase 3 (red) embedded in matrix of Phase 1 used for Example 2. [Color figure can be viewed at wileyonlinelibrary.com]

where $E_{\mathrm{Q,est}}$ is a "worst case" combination of the upper and lower bounds, and E_{Q} the exact error in the quantity of interest.

6.1 | Example 1: Isotropic RVE with a single centered inclusion

As a first example, we consider an isotropic RVE of size $1\,\mathrm{m} \times 1\,\mathrm{m} \times 1\,\mathrm{m}$, with a single centered inclusion with radius $0.4\,m$, see Figure 1. For this example, we use the same load case as in the training computations (see Section 6.1.1) for the prediction; the $\bar{\epsilon}_{11}$ component is rapidly increased and then kept constant, while keeping the other strain components at 0.

6.1.1 | Example 1: Identification of reduced basis

The snapshots for the POD are extracted from training computations. For the first example, we perform a stress-relaxation test as training by ramping up $\bar{\epsilon}_{11}(t) = \overline{\psi}(t)$ according to Figure 2, while keeping the other components at 0. The resulting homogenized stress is plotted in Figure 3. The snapshots for the POD are collected from the "relaxation part", i.e. from the time steps where $t > 1 \times 10^{-5}$s. In Figure 4 the first two POD modes are plotted, together with the first SD modes for the RVE.

6.1.2 | Example 1: Energy norm of the error

The estimated error in energy norm, E_{est}, given in Equation (77), is plotted in Figure 5 for the prediction load case (which, for this example is the same as the training load case). The exact error, $E = \|g\|$, is also plotted in the same figure. We note
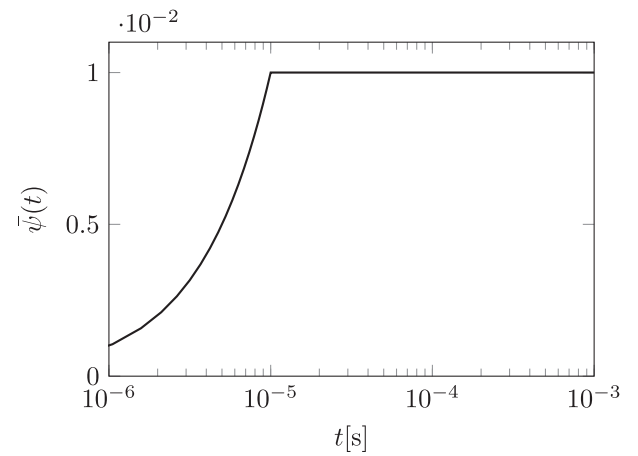
FIGURE 2 Ramp function used for prescribing macroscale strain components for the training computation(s)
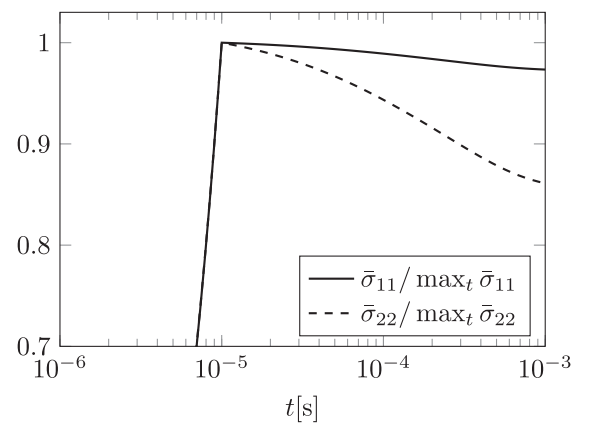
FIGURE 3 *Example 1:* Homogenized stress, normalized with their peak values, from the fully resolved solution with the load case used for the training computation(s)
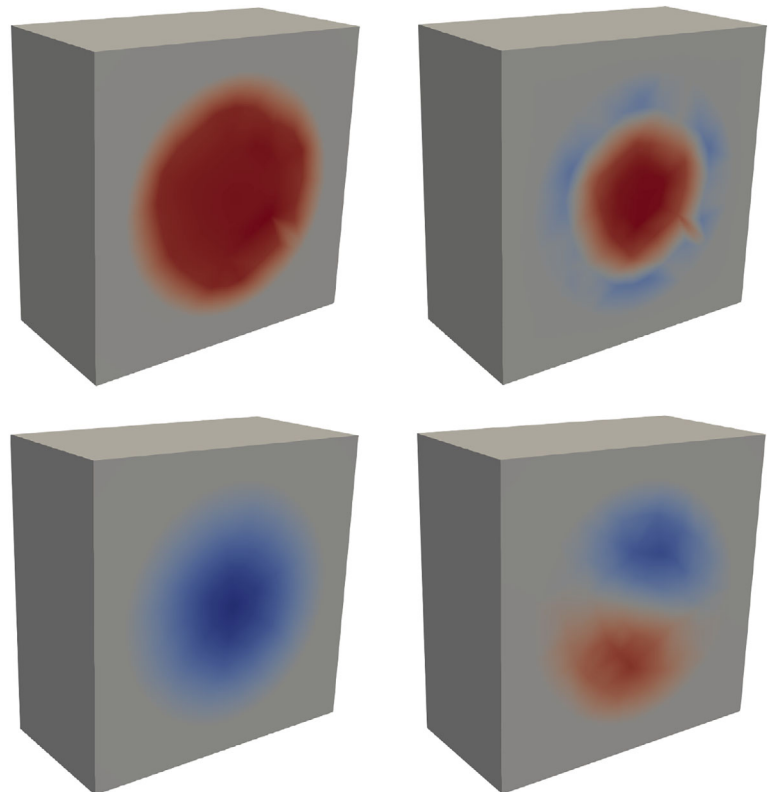
FIGURE 4 *Example 1:* First and second POD modes (top left and top right, respectively) resulting from the training computations, together with the first and second SD modes (bottom left and bottom right, respectively) visualized on a cut plane through the middle of the RVE. [Color figure can be viewed at wileyonlinelibrary.com]
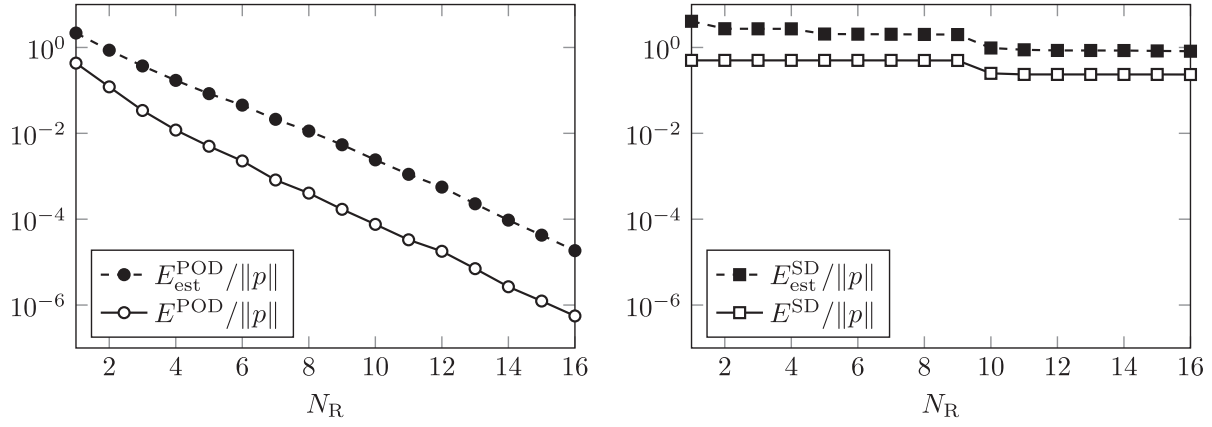
FIGURE 5 *Example 1:* Exact and estimated error in energy norm using the POD (left) and SD (right) basis
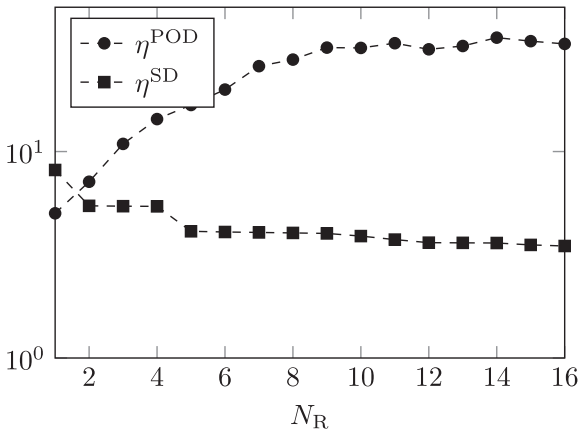
FIGURE 6 *Example 1:* Effectivity index for the estimated error in energy norm

that, as expected, the residual, and therefore also the error estimate, decreases much faster for the POD base compared with the SD base. The effectivity index, η, for the estimate in energy norm is plotted in Figure 6. We note that the effectivity index increases quickly for the POD base, but stays rather constant for the SD base. One explanation for this is the fact that, with the SD base, we can use a higher eigenvalue for the final estimate, as discussed in Section 4.4.2.

6.1.3 | Example 1: Error in time-averaged homogenized stress

In Section 5, we discussed how to estimate the error in a user-defined quantity of interest, and in particular the homogenized stress. We now consider the time-averaged homogenized stress, $\overline{\sigma}_{11}$, as the quantity of interest and compute the upper and lower estimates for the error, $E_{Q,est}^{+}$ and $E_{Q,est}^{-}$, given in Equation (121). The results are plotted in Figure 7, and the combined estimate, from Equation (123), is plotted in Figure 8. In both figures, we also include the exact error, E_Q, as compared with the full finite element solution. We note that the behavior of the estimates, and the corresponding effectivity indexes in Figure 9, is very similar to the estimate of the energy norm from the previous section. However, in Figure 9, we see that the effectivity index deteriorates even more for the POD estimate.

6.2 | Example 2: Heterogeneous RVE with multiple inclusions

For the second example, we consider an RVE of size $1\,\text{m} \times 1\,\text{m} \times 1\,\text{m}$, with multiple, nonoverlapping, spherical inclusions with radii between 0.1 and 0.4 m, see Figure 1. For the prediction, we combine prescribed macroscale strain in 11, 22, and 33 directions according to Figure 10, resulting in macroscale stresses presented in Figure 11.
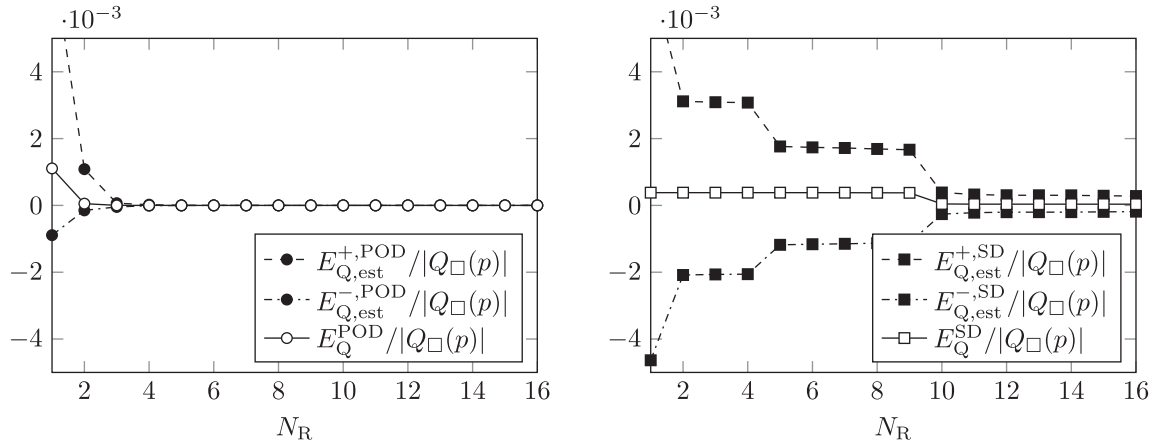
FIGURE 7 *Example 1:* Exact error and upper and lower estimates of the error in time-averaged homogenized stress for the POD (left) and SD (right) basis
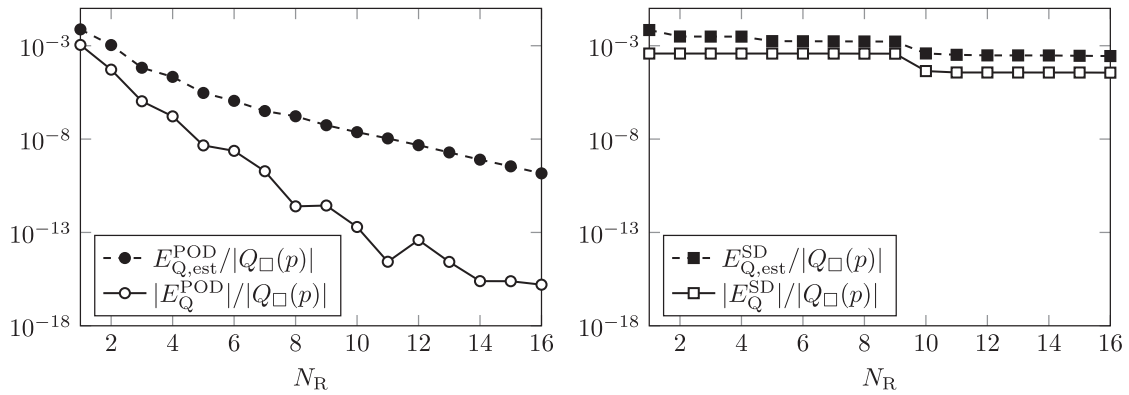
FIGURE 8 *Example 1:* Exact error and the combined estimate $E_{Q,est}$ of the error in time-averaged homogenized stress for the POD (left) and SD (right) basis

FIGURE 9 *Example 1:* Effectivity index for the estimated error in time-averaged homogenized stress
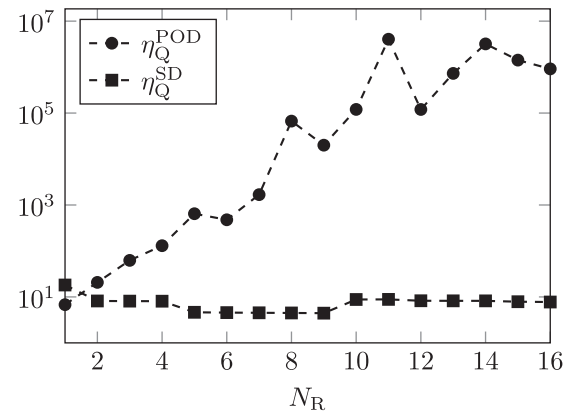
6.2.1 | Example 2: Identification of reduced basis

For the second example, we also use the stress relaxation test from Section 6.1.1, but now in three directions by setting $\overline{\varepsilon}_{ii}(t) = \overline{\psi}(t)$, for $i = 1,2,3$, resulting in three training computations from which we collect snapshots. The resulting first two POD modes are plotted in Figure 12, together with the first two SD modes.
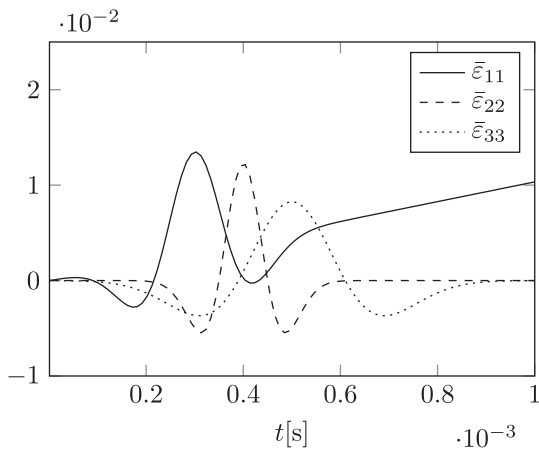
FIGURE 10 *Example 2:* Prescribed macroscale strains, as functions of time, defining the load case used for prediction
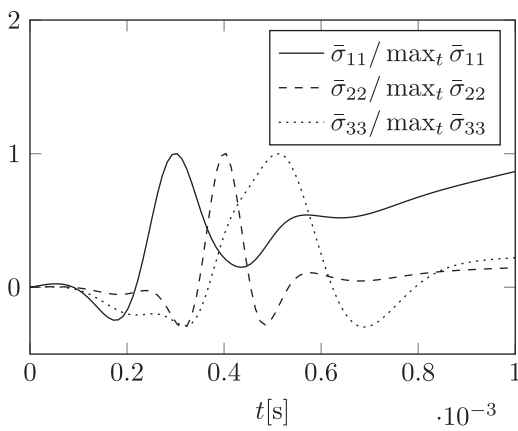
FIGURE 11 *Example 2:* Homogenized stress, normalized with their peak values, from the fully resolved solution for the load case used for prediction
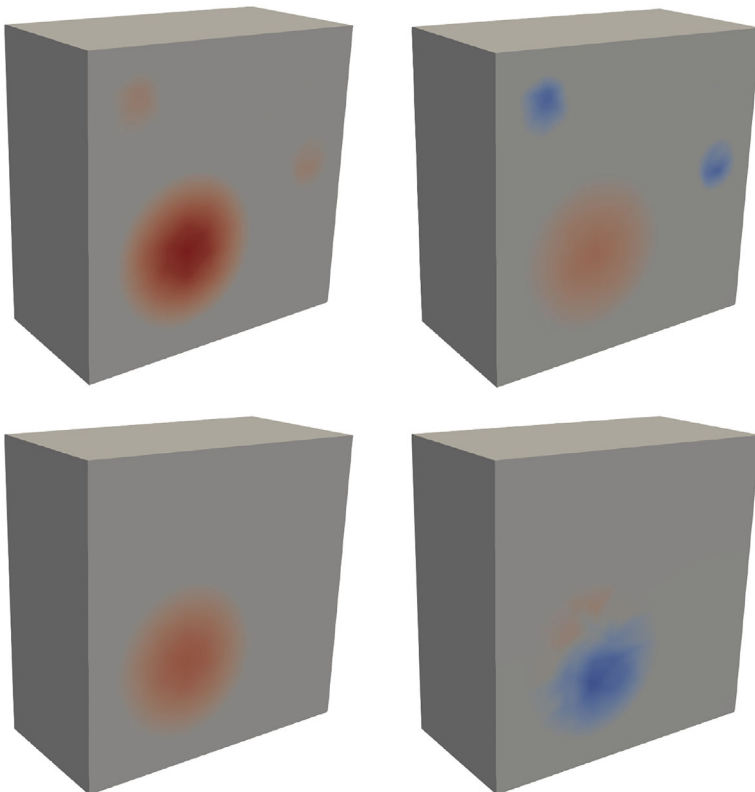
FIGURE 12 *Example 2:* First and second POD modes (top left and top right, respectively) resulting from the training computations, together with the first and second SD modes (bottom left and bottom right, respectively) visualized on a cut plane through the middle of the RVE [Color figure can be viewed at wileyonlinelibrary.com]
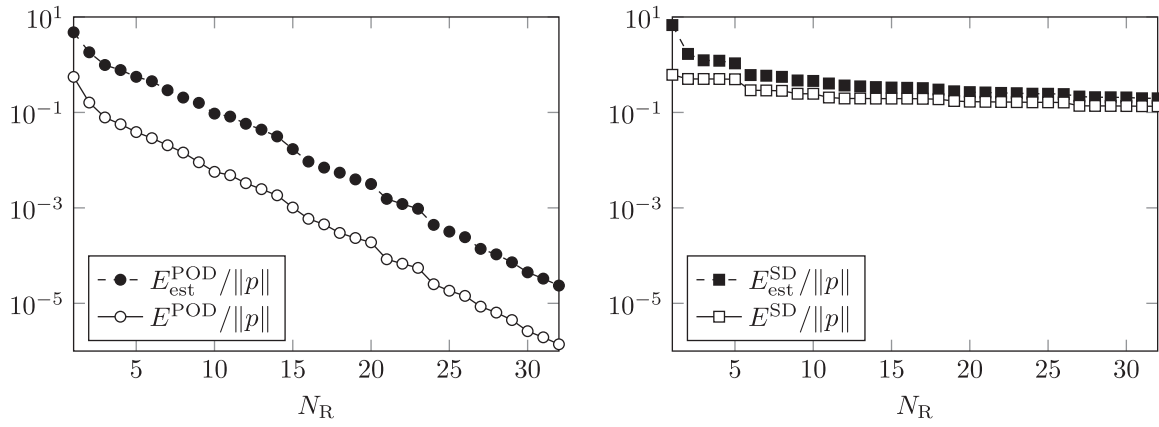
FIGURE 13 *Example 2:* Exact and estimated error in energy norm using the POD (left) and SD (right) basis

FIGURE 14 *Example 2:* Effectivity index for the estimated error in energy norm
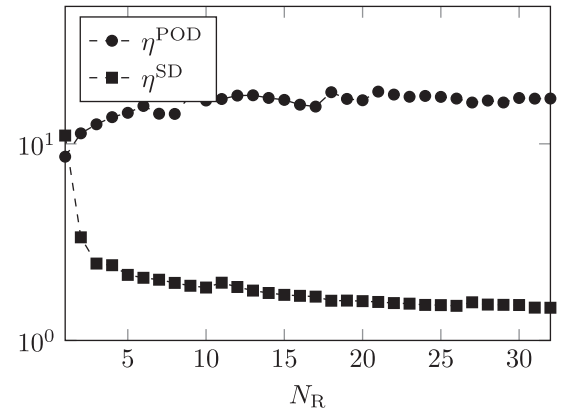
6.2.2 | Example 2: Energy norm of the error

The estimated error in energy norm, E_{est}, given in Equation (77), is plotted in Figure 13, together with the exact error, $E = \|g\|$. We note that the result is similar to the results for the first example in the previous section. In particular, we note that, as expected, the residual, and therefore also the error estimate, decreases much faster for the POD base compared with the SD base. The effectivity index, η, for the estimate in energy norm is plotted in Figure 14. We note that the effectivity index is higher for the POD base than for the SD base, just as for the previous example.

6.2.3 | Example 2: Error in time-averaged homogenized stress

Once again we use the time average of $\overline{\sigma}_{11}$ as the quantity of interest for the goal oriented error estimation. The resulting upper and lower bounds, $E_{Q,\text{est}}^+$ and $E_{Q,\text{est}}^-$ from Equation (121), are plotted in Figure 15, together with the combined estimate and effectivity index (123) plotted in Figures 16 and 17, respectively. The results are similar to the first example, where the POD base results in much smaller residual and hence smaller estimate, but the spectral base results in a better effectivity index.

6.3 | Example 3: Influence of training data

In the third numerical example, we investigate the effect of the training data on the error estimate. The training data are collected using the same method as for the previous example (see Section 6.2.1), however, we vary the activation function
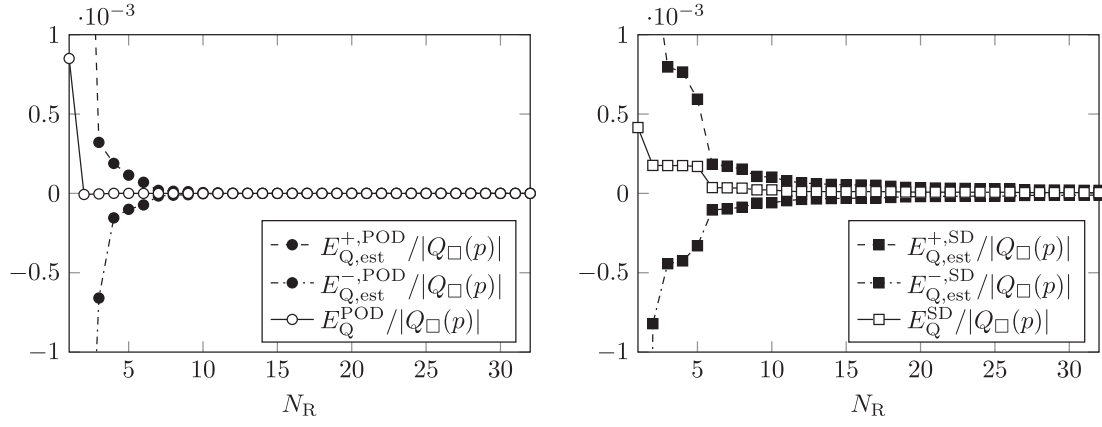
FIGURE 15 *Example 2:* Exact error and upper and lower estimates of the error in time-averaged homogenized stress for the POD (left) and SD (right) basis
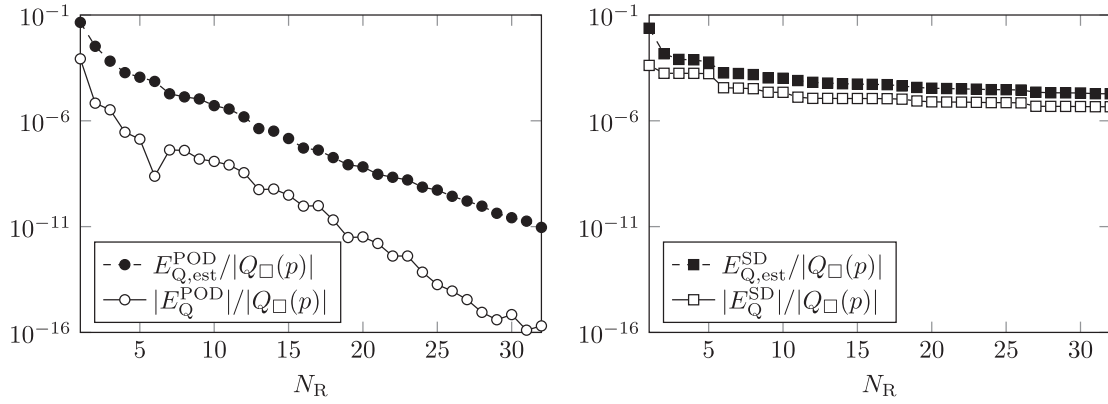

FIGURE 16 *Example 2:* Exact error and the combined estimate $E_{\mathrm{Q,est}}$ of the error in time-averaged homogenized stress for the POD (left) and SD (right) basis
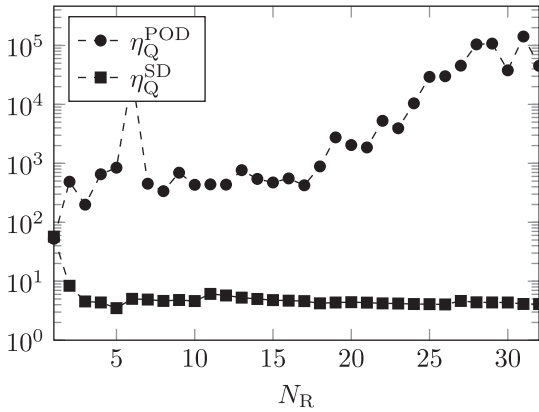

**FIGURE 17** *Example 2:* Effectivity index for the estimated error in time-averaged homogenized stress

$\overline{\psi}$ as follows:

$$\overline{\psi}_1(t) = \overline{\psi}(t), \tag{124a}$$

$$\overline{\psi}_2(t) = \overline{\psi}(t/10), \tag{124b}$$

$$\overline{\psi}_3(t) = \overline{\psi}(10t), \tag{124c}$$

FIGURE 18 *Example 3:* Threshold number of modes N_R required for reaching 10%, 1%, 0.1%, and 0.01% estimated relative error in terms of the energy norm, respectively, for the three different POD basis constructed from the datasets DS1, DS2, and DS3
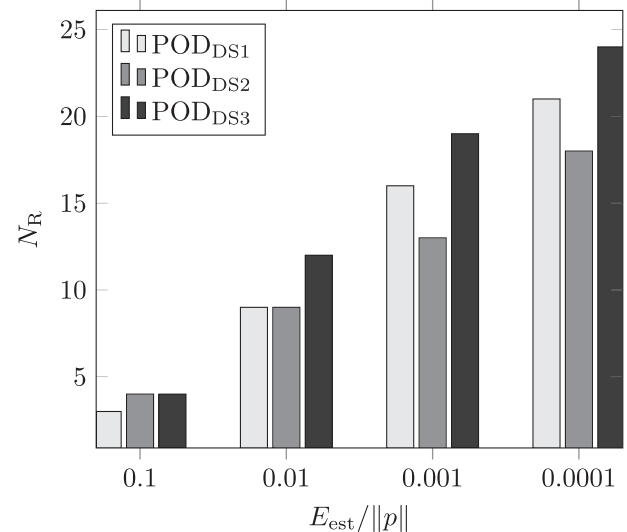
in order to obtain three different datasets (DS1, DS2, DS3) to build the POD basis from. The microstructure of the RVE, and the load case used for the prediction, are the same as in Example 2.

In Figure 18, we illustrate the threshold number of modes needed in order to obtain a certain accuracy, in terms of the energy norm, indicated by the estimate. We note that the threshold differs between the different datasets quite a lot even for this simple load case.

This example also illustrates the need for different number of modes, or even different basis, for different macroscopic location in an FE^2 setting where the loading are different for each RVE computation.

7 | CONCLUSIONS AND OUTLOOK

In this article, we have presented an a posteriori error estimate for the error introduced by NMR in the context of homogenization of porous media. More specifically, we extended the reduced order model presented in Jänicke et al[12] with an explicit, fully computable, and computationally efficient error estimator for guaranteed bounds of the error in terms of (i) energy norm and (ii) user-defined QoI. The estimator is a generalization of similar estimators presented by the authors[23,24] with the major important differences that it handles the coupled problem, and that the estimator is derived for a POD basis rather than an SD basis.

The performance of the estimator was demonstrated by two numerical examples, and for reduced basis obtained by (i) SD and (ii) POD. As expected, the POD base results in much smaller residuals compared with the SD base, but in general the effectivity index of the estimator when using an SD base is better. It is noted that the sharpness of the estimator quickly deteriorates with increasing number of modes. However, considering the fact that the estimates are fully computable with negligible overhead, a sharper estimate would probably require significantly higher computational cost.

An interesting extension, left for future work, would be to develop a method to create a mixed base by combining spectral modes and POD modes in a clever way, in order to reduce the high effectivity index obtained from the estimator for the pure POD case.

As to future work, the obvious next step is to embed the error estimator for the subscale problem, presented in this article, into a full-fledged nested FE^2 procedure. This would require taking care of error transport between the two scales, similar to what was presented in Ekre et al[24] for the linear heat flow problem. We also, once again, note that in this work we completely ignored errors from sources such as time and space discretization, and it would be of interest to extend the estimator with the ability to estimate those errors as well. Finally, we note that we have not considered adaptive techniques in this article. It would be interesting to investigate this, and use the error estimator as a measure for adaptively adding new modes to the subscale problem on the fly.

ORCID

Fredrik Ekre https://orcid.org/0000-0003-2476-5406
Fredrik Larsson https://orcid.org/0000-0002-7786-5040
Kenneth Runesson https://orcid.org/0000-0003-1714-4994
Ralf Jänicke http://orcid.org/0000-0001-8816-6643

REFERENCES

1. Larsson Fredrik, Runesson Kenneth. Adaptive bridging of scales in continuum modeling based on error control. *Int J Multiscale Comput Eng*. 2008;6:371-392. https://doi.org/10.1615/IntJMultCompEng.v6.i4.80.
2. Larsson F, Runesson K. On two-scale adaptive FE analysis of micro-heterogeneous media with seamless scale-bridging. *Comput Methods Appl Mech Eng*. 2011;200(37):2662-2674. https://doi.org/10.1016/j.cma.2010.10.012.
3. Fish J, Yuan Z. Multiscale enrichment based on partition of unity for nonperiodic fields and nonlinear problems. *Comput Mech*. 2007;40(2):249-259. https://doi.org/10.1007/s00466-006-0095-0.
4. Oskay C, Fish J. On calibration and validation of eigendeformation-based multiscale models for failure analysis of heterogeneous systems. *Comput Mech*. 2008;42(2):181-195. https://doi.org/10.1007/s00466-007-0197-3.
5. Dvorak GJ, Benveniste Y. On transformation strains and uniform fields in multiphase elastic media. *Proc R Soc Lond A Math Phys Sci*. 1992;437(1900):291-310. https://doi.org/10.1098/rspa.1992.0062.
6. Michel JC, Suquet P. Nonuniform transformation field analysis. *Int J Solids Struct*. 2003;40(25):6937-6955. https://doi.org/10.1016/S0020-7683(03)00346-9.
7. Michel JC, Suquet P. Computational analysis of nonlinear composite structures using the nonuniform transformation field analysis. *Comput Methods Appl Mech Eng*. 2004;193(48):5477-5502. https://doi.org/10.1016/j.cma.2003.12.071.
8. Fritzen F, Böhlke T. Reduced basis homogenization of viscoelastic composites. *Compos Sci Technol*. 2013;76:84-91. https://doi.org/10.1016/j.compscitech.2012.12.012.
9. Fritzen F, Leuschner M. Reduced basis hybrid computational homogenization based on a mixed incremental formulation. *Comput Methods Appl Mech Eng*. 2013;260:143-154. https://doi.org/10.1016/j.cma.2013.03.007.
10. Fritzen F, Hodapp M, Leuschner M. GPU accelerated computational homogenization based on a variational approach in a reduced basis framework. *Comput Methods Appl Mech Eng*. 2014;278:186-217. https://doi.org/10.1016/j.cma.2014.05.006.
11. Fritzen F, Leuschner M. Nonlinear reduced order homogenization of materials including cohesive interfaces. *Comput Mech*. 2015;56(1):131-151. https://doi.org/10.1007/s00466-015-1163-0.
12. Jänicke R, Larsson F, Runesson K, Steeb H. Numerical identification of a viscoelastic substitute model for heterogeneous poroelastic media by a reduced order homogenization approach. *Comput Methods Appl Mech Eng*. 2016;298:108-120. https://doi.org/10.1016/j.cma.2015.09.024.
13. Nguyen NC. A multiscale reduced-basis method for parametrized elliptic partial differential equations with multiple scales. *J Comput Phys*. 2008;227(23):9807-9822. https://doi.org/10.1016/j.jcp.2008.07.025.
14. Efendiev Y, Galvis J, Thomines F. A systematic coarse-scale model reduction technique for parameter-dependent flows in highly heterogeneous media and its applications. *Multiscale Model Simulat*. 2012;10(4):1317-1343. https://doi.org/10.1137/110853030.
15. Efendiev Y, Galvis J, Gildin E. Local–global multiscale model reduction for flows in high-contrast heterogeneous media. *J Comput Phys*. 2012;231(24):8100-8113. https://doi.org/10.1016/j.jcp.2012.07.032.
16. Hernández JA, Oliver J, Huespe AE, Caicedo MA, Cante JC. High-performance model reduction techniques in computational multiscale homogenization. *Comput Methods Appl Mech Eng*. 2014;276:149-189. https://doi.org/10.1016/j.cma.2014.03.011.
17. Memarnahavandi A, Larsson F, Runesson K. A goal-oriented adaptive procedure for the quasi-continuum method with cluster approximation. *Comput Mech*. 2015;55(4):617-642. https://doi.org/10.1007/s00466-015-1127-4.
18. Abdulle A, Bai Y, Vilmart G. Reduced basis finite element heterogeneous multiscale method for quasilinear elliptic homogenization problems. *Discr Continu Dyn Syst Ser S*. 2015;8(1):91-118. http://www.aimsciences.org/journals/displayArticlesnew.jsp?paperID=101022014.
19. Abdulle A, Bai Y. Adaptive reduced basis finite element heterogeneous multiscale method. *Comput Methods Appl Mech Eng*. 2013;257:203-220. https://doi.org/10.1016/j.cma.2013.01.002.
20. Boyaval S. Reduced-basis approach for homogenization beyond the periodic setting. *Multiscale Model Simulat*. 2008;7(1):466-494. https://doi.org/10.1137/070688791.

[9] https://github.com/KristofferC/JuAFEM.jl

21. Kerfriden P, Ródenas JJ, Bordas SP-A. Certification of projection-based reduced order modelling in computational homogenisation by the constitutive relation error. *Int J Numer Methods Eng*. 2014;97(6):395-422. https://doi.org/10.1002/nme.4588.

22. Chamoin L, Legoll F. A posteriori error estimation and adaptive strategy for the control of MsFEM computations. *Comput Methods Appl Mech Eng*. 2018;336:1-38. https://doi.org/10.1016/j.cma.2018.02.016.

23. Aggestam E, Larsson F, Runesson K, Ekre F. Numerical model reduction with error control in computational homogenization of transient heat flow. *Comput Methods Appl Mech Eng*. 2017;326:193-222. https://doi.org/10.1016/j.cma.2017.08.006.

24. Ekre F, Larsson F, Runesson K. On error controlled numerical model reduction in FE2-analysis of transient heat flow. *Int J Numer Methods Eng*. 2019;119(1):38-73. https://doi.org/10.1002/nme.6041.

25. Parés N, Díez P, Huerta A. Bounds of functional outputs for parabolic problems. Part I: exact bounds of the discontinuous Galerkin time discretization. *Comput Methods Appl Mech Eng*. 2007;197(19):1641-1660. https://doi.org/10.1016/j.cma.2007.08.025.

26. Parés N, Díez P, Huerta A. Bounds of functional outputs for parabolic problems. Part II: bounds of the exact solution. *Comput Methods Appl Mech Eng*. 2007;197(19):1661-1679. https://doi.org/10.1016/j.cma.2007.08.024.

27. Parés N, Díez P, Huerta A. Exact bounds for linear outputs of the advection-diffusion-reaction equation using flux-free error estimates. *SIAM J Sci Comput*. 2009;31(4):3064-3089. https://doi.org/10.1137/080724356.

28. Jakobsson H, Bengzon F, Larson MG. Adaptive component mode synthesis in linear elasticity. *Int J Numer Methods Eng*. 2011;86(7):829-844. https://doi.org/10.1002/nme.3078.

29. Oden JT, Prudhomme S. Goal-oriented error estimation and adaptivity for the finite element method. *Comput Math Appl*. 2001;41(5):735-756. https://doi.org/10.1016/S0898-1221(00)00317-5.

30. Biot MA. General theory of three-dimensional consolidation. *J Appl Phys*. 1941;12(2):155-164. https://doi.org/10.1063/1.1712886.

31. Rice JR, Cleary MP. Some basic stress diffusion solutions for fluid-saturated elastic porous media with compressible constituents. *Rev Geophys*. 1976;14(2):227. https://doi.org/10.1029/RG014i002p00227.

32. Larsson F, Runesson K, Su F. Variationally consistent computational homogenization of transient heat flow. *Int J Numer Methods Eng*. 2010;81(13):1659-1686. https://doi.org/10.1002/nme.2747.

33. Bezanson J, Edelman A, Karpinski S, Shah V. Julia: a fresh approach to numerical computing. *SIAM Rev*. 2017;59(1):65-98. https://doi.org/10.1137/141000671.

34. Carlsson K, Ekre F. Tensors.jl – tensor computations in Julia. *J Open Res Softw*. 2019;7(1):1-5. https://doi.org/10.5334/jors.182.

35. Geuzaine C, Remacle J-F. Gmsh: a 3-D finite element mesh generator with built-in pre- and post-processing facilities. *Int J Numer Methods Eng*. 2009;79(11):1309-1331. https://doi.org/10.1002/nme.2579.

SUPPORTING INFORMATION

Additional supporting information may be found online in the Supporting Information section at the end of this article.